Formation and decay of a tributary-dammed lake, Laonong River, Taiwan

Hervé Capart,[1] Jammie P. C. Hsu,[1,2] Steven Y. J. Lai,[1] and Meng-Long Hsieh[3]

Received 29 January 2010; revised 4 July 2010; accepted 12 July 2010; published 13 November 2010.

[1] We use field observations, laboratory experiments, and mathematical theory to characterize the full life cycle of a tributary-dammed lake. The natural lake formed in August 2007 at the confluence of the Laonong River, southern Taiwan, with a steep tributary. Due to heavy rains from typhoons Wutip and Sepat, the tributary delivered massive amounts of sediment to the confluence. This caused damming of the trunk river, the growth of a lake, and the demise of a bridge upstream of the confluence. The lake lasted until October 2007, gradually decaying due to incision and infill by subsequent stream flow. We reconstruct the episode using hydrological records, ground observations, and surveyed profiles. We then use the event to verify a mathematical theory of river and lake bed evolution. The theory is based on a diffusion description of river morphodynamics, constrained by backwater effects due to lake formation. After validation using laboratory experiments, the theory is applied to the Laonong field event. Good agreement is obtained between calculated and surveyed long profiles. The theory can also reproduce the complex stage hydrograph recorded upstream of the confluence. This suggests a role for simplified, but laboratory-tested mathematical theory in quantitative investigations of fluvial processes in the field.

Citation: Capart, H., J. P. C. Hsu, S. Y. J. Lai, and M.-L. Hsieh (2010), Formation and decay of a tributary-dammed lake, Laonong River, Taiwan, *Water Resour. Res.*, *46*, W11522, doi:10.1029/2010WR009159.

1. Introduction

[2] In nonglaciated valleys, natural lakes most commonly form as a direct or indirect consequence of landslides [*Hutchinson*, 1957]. A landslide-dammed lake forms when a valley side directly slumps into a river [*Costa and Schuster*, 1988; *Chen*, 1999]. Landslides can also cause lake formation in a more indirect manner, by contributing large volumes of loose material to headwater streams. The products of mass wasting can then be mobilized by torrential or debris flows, and conveyed down tributary valleys to their confluences with trunk rivers [*Benda et al.*, 2004; *Lancaster and Casebeer*, 2007]. A tributary-dammed lake forms when the resulting confluence aggradation is sufficiently rapid [*Lane*, 1955; *Hsu and Capart*, 2008]. Various contemporary river and lake profiles have been attributed to ancient tributary-damming episodes [*Galay et al.*, 1983; *Wright et al.*, 1998; *Blumentritt et al.*, 2009].

[3] In a previous study [*Hsu and Capart*, 2008], we proposed a simple mathematical theory describing the response of alluvial rivers to sediment influx from tributaries. The theory is based on a diffusion description of river morphodynamics, constrained by backwater effects. The theory yields a criterion for the occurrence of tributary-dammed lakes, and analytical solutions for the coevolving river and lake profiles. It predicts that a tributary-dammed lake will form if the sediment influx from the tributary exceeds twice the background bed load transit in the trunk river. Below this threshold, tributary sediment influx causes a cuspate, symmetric aggradation of the trunk river, without forming a lake. Above the threshold, an asymmetric aggradation is predicted upstream and downstream of an expanding lake. This theory was checked quantitatively against idealized laboratory experiments [*Hsu*, 2007]. Field verification, however, could not be performed due to lack of adequate data.

[4] In August 2007, heavy rains brought by typhoons Wutip and Sepat triggered sustained debris flows in a steep tributary of the Laonong River, southern Taiwan. The resulting massive influx of sediment formed a dam at the tributary confluence, causing a lake to grow and drown the upstream reaches of the trunk river (Figure 1). The lake lasted into October 2007, gradually decaying due to subsequent stream flow. We had the opportunity to observe the lake before its decay. We were also able to collect unusually complete data regarding the whole life cycle of the lake, including measurements acquired by the Taiwan Water Resources Agency (WRA) and by a field survey we conducted in February 2008. The data include hydrological records and topographic transects acquired before and after the lake formation episode. The event thus provides a unique opportunity to verify our mathematical theory of river and lake evolution.

[5] To simulate the Laonong episode, it is necessary to extend the theory beyond the analytical model proposed in *Hsu and Capart* [2008]. In field conditions, more compli-

[1]Department of Civil Engineering and Hydrotech Research Institute, National Taiwan University, Taipei, Taiwan.
[2]Now at Fifth River Management Office, Water Resources Agency, Ministry of Economic Affairs, Chiayi City, Taiwan.
[3]Department of Earth and Environmental Sciences, National Chung Cheng University, Chiayi County, Taiwan.

0043-1397/10/2010WR009159

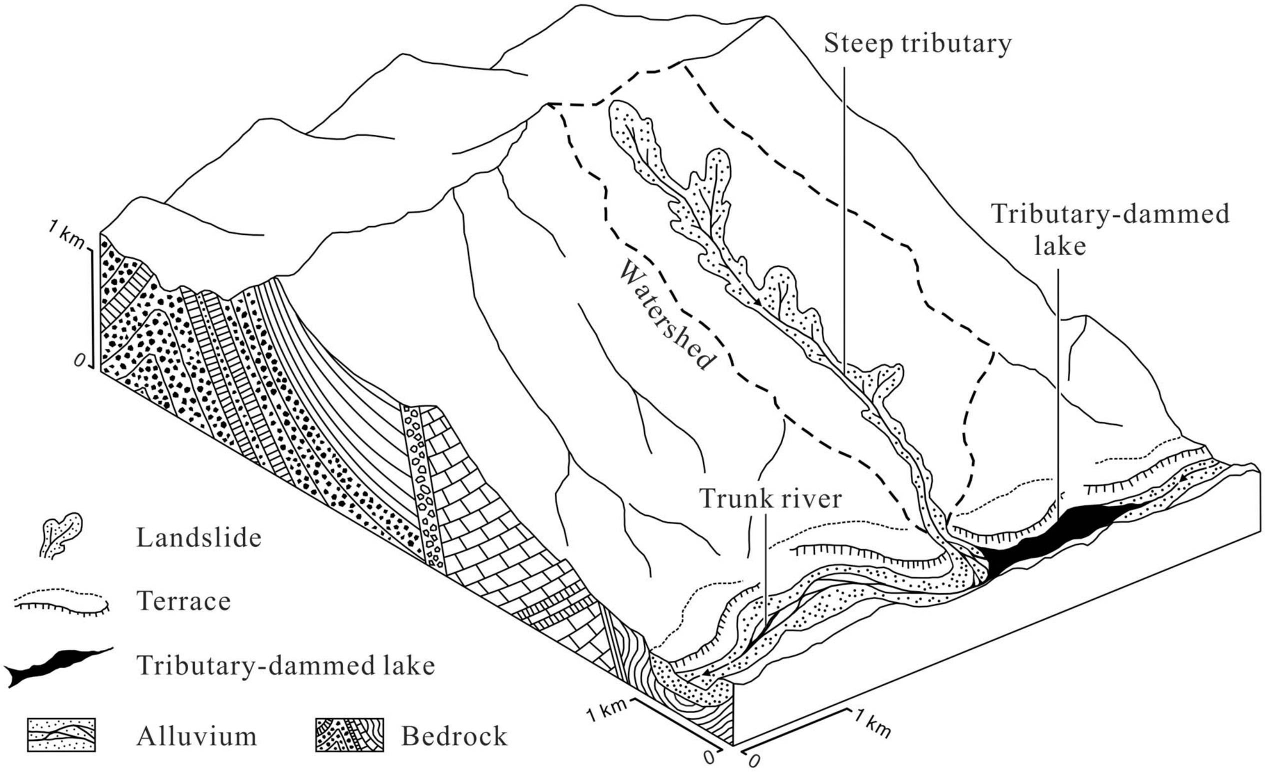

Figure 1. Schematic of the natural lake formed in August 2007 at the confluence of a steep tributary (Pu-tun-pu-nas River) with a semialluvial trunk river (Laonong River), southern Taiwan. The tributary drains a small watershed, highly prone to landslides and debris flows, which contributed large amounts of sediment to the trunk river. This caused confluence aggradation and the formation of a tributary dam across the trunk river. Other episodes of massive sediment supply from this tributary have occurred in the past, as recorded by the high fan terraces bordering the confluence, and occurred again more recently due to record-breaking rains from Typhoon Morakot in August 2009. The geological cross section is drawn after *Water Resources Agency* [1997].

cated circumstances must be taken into account, including the highly unsteady river discharge associated with typhoon floods. Because the 2007 Laonong episode involved the full life cycle of a tributary-dammed lake, our model of lake initiation and growth must also be extended to simulate lake decay and disappearance. As a result, the governing equations of the theory need to be solved numerically instead of analytically.

[6] In this paper, we summarize our observations of the 2007 tributary-dammed lake. We present the data analysis performed to reconstruct the evolution of the river bed and water level at different stages of the lake life cycle. Next, we explain the bases of our theory, and how solutions are calculated. To check the numerical model, we compare model results with analytical solutions (for lake growth) and laboratory experiments (for the full lake life cycle). Finally, we apply the model to the Laonong River and verify that the theory can reproduce the observed river and lake evolution.

[7] Our work has various implications of possible relevance to river engineers and Earth scientists. First, our case study highlights the possibility that swings in bed elevation due to tributary disturbances may greatly exceed water depth changes due to discharge variations. The common engineering practice of estimating the design water stage using the current river bed elevation plus the expected water depth for a discharge of a certain return period may therefore greatly underestimate flood risk. The study may also aid disaster mitigation efforts by providing estimates of the possible magnitude and lifetime of natural damming events. Of interest to Earth scientists, our analysis may help interpret ancient episodes preserved in the sedimentary record. The back analysis of individual events, as performed in the present paper, further shows potential as a way to quantify rates of coarse sediment production and transport in watersheds where only the suspended load of fine sediment can be directly measured.

2. Study Site and Lake Observations

2.1. Setting

[8] The south flowing Laonong River, with a watershed area of ~2000 km^2, is a major tributary of the Kaoping River that drains mountains up to 4000 m high in southwestern Taiwan (Figure 2). Except for its lowest 20 km long course that flows on the Pintung Plain, the Laonong River runs between the main divide of the Central Range (the backbone range of Taiwan Island) to the east and the secondary Yu-shan Range to the west (Figure 2a). The lower half of this mountain river course flows roughly along a fault zone separating the metamorphosed rock

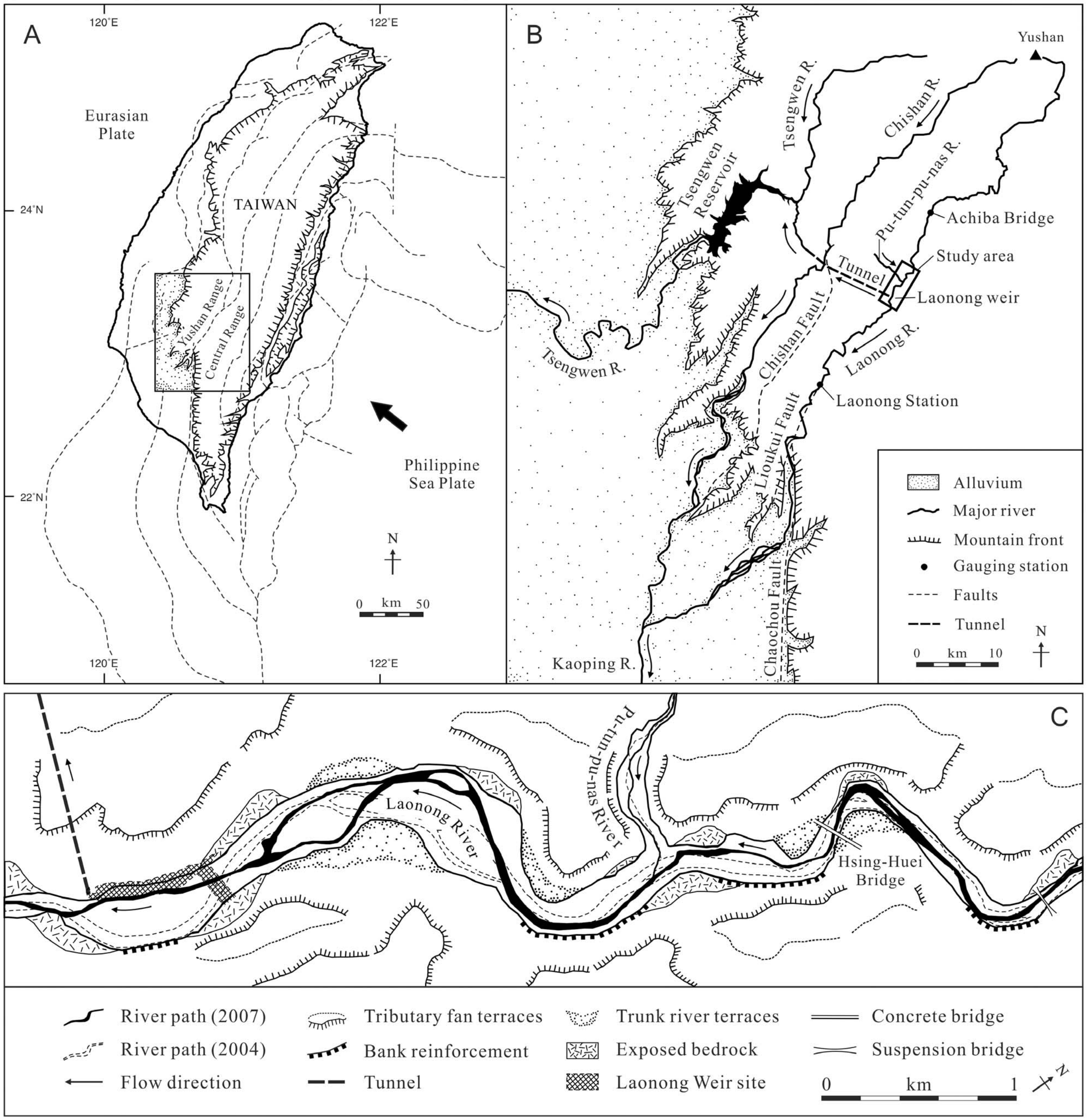

Figure 2. Setting of the field study. (a) Taiwan Island; (b) Laonong River Basin; and (c) confluence between the Laonong and Pu-tun-pu-nas rivers. Faults in Figure 2a drawn after *Malavieille and Trullenque* [2009]. In Figure 2c, terraces are drawn after *Hsieh and Chyi* [2010], and the bank classification is based on air photos and ground observations.

formations (argillite, slate, metasandstone) underlying the Central Range from the sandstone/shale formations constituting the Yu-shan Range. This fault-bounded river reach is relatively straight, and flanked by a series of river terraces. As the river reach is also relatively wide and gentle, it provides optimal locations for the formation of tributary fans. Almost all tributaries joining this trunk river reach develop alluvial or debris fans. Most of them, however, have been abandoned and incised by the trunk river, forming fan terraces of various sizes and heights. These fan terraces, up to 200 m high above the trunk river, document episodic activities of landslides and debris flows in tributary watersheds and are among the most spectacular landforms exhibited in Taiwan's mountains [*Lin*, 1957; *Hsieh and Chyi*, 2010].

[9] The Laonong watershed experiences a tropical–subtropical monsoon climate, receiving annual rainfall of 2000–4000 mm. The resulting mean annual discharge at the Laonong gauging station, where the river emanates from mountains, is approximately 60 m^3 s^{-1}. Rainfall comes mainly from the summer monsoon and from tropical typhoons and shows strong seasonality. At the Laonong gauging station (Figure 2b), mean monthly discharges fall in

Figure 3. Formation and decay of a lake at the confluence of the Pu-tun-pu-nas River with the Laonong River. (a) Tributary fan on 10 June 2005; (b) raised fan surface on 26 September 2007; (c) tributary-dammed lake viewed from upstream of the confluence on 26 September 2007; (d) drained lake bed on 6 January 2008; (e) Hsing-huei Bridge, 1 km upstream of the confluence, on 24 October 2006 (used with permission from Southern Region Water Resources Office, Water Resource Agency of Taiwan); and (f) bridge site on 26 September 2007. The bridge deck has been washed away, but the central pile and lateral abutments remain.

the ranges 50–170 and 15–40 $m^3\ s^{-1}$ during the wet (May–October) and dry seasons, respectively [*Shiau and Wu*, 2009]. Individual flood peaks associated with typhoon events can reach daily discharges as high as 1000 $m^3\ s^{-1}$.

[10] The active channels and floodplains characterizing the mountain course of the Laonong River are confined laterally by bedrock and, occasionally, by sedimentary fluvial or fan terraces. Bedrock, however, is rarely exposed

Figure 4. Panoramic views of the Pu-tun-pu-nas tributary dam at various stages of degradation, viewed from the opposite bank of the Laonong River. (a) During lake decay on 26 September 2007; (b) after complete drainage of the lake on 6 January 2008; and (c) after Typhoon Kalmaegi, on 23 July, 2008. Flow in the trunk river is from right to left.

along the bed of the lower, fault-bounded portion of the Laonong River, even during low-flow conditions. Instead, the bedrock floor of this relatively wide and gentle river is buried under alluvial cover. Drilling performed by the WRA 3 km downstream of our study site reveals bedrock at depths of 10–20 m beneath the alluvium. The current lower mountain portion of the Laonong River may thus be considered semialluvial [*Brooks and Lawrence*, 1999]: Valley sides are confined mainly by bedrock, but the valley bottom consists of alluvial fill of significant thickness.

[11] Among the tributaries of the Laonong River, the most prone to episodic landslides and debris flows is probably the Pu-tun-pu-nas River (Figure 1). This is a steep tributary (relief, 1500 m; mean gradient, 0.3) draining the Yu-shan Range. It has a drainage area of 6.2 km^2, two orders of magnitude smaller than the contributing area of 542 km^2 of the trunk river upstream from their confluence. Although it contributes only a very small fraction of the total water discharge, this tributary constitutes a major source of sediment supply to the Laonong River. Ancient sediment supply episodes are manifested by elevated fan terraces surrounding the confluence, which yield multiple radiocarbon ages ranging from 6500 to 1400 years before present [*Hsieh and Chyi*, 2010]. Since the 1980s, we have observed repeated

Table 1. Reconstructed Timeline of the 2007 Lake Formation and Decay Episode at the Confluence of the Laonong and Pu-tun-pu-nas Rivers, Southern Taiwan

Date	*t* (day)	Event or Observation	Origin of Information
1-5-2007	0	Beginning of the 2007 typhoon season	By convention
8-8-2007	99	Streamflow increase due to Typhoon Wutip	Streamflow at upstream and downstream stations
8-8-2007	99	Start of period of debris flow activity in Pu-tun-pu-nas River	Deduced from best fit of simulation results
13-8-2007	104	Peak discharge of Typhoon Wutip	Streamflow at upstream and downstream stations
19-8-2007	110	Peak discharge of Typhoon Sepat	Streamflow at upstream and downstream stations
19-8-2007	110	Last stage record at Hsing-huei Bridge	Water Resources Agency
15-9-2007	137	End of period of debris flow activity in Pu-tun-pu-nas River	Deduced from best fit of simulation results
19-9-2007	141	Peak discharge of Typhoon Wipha	Streamflow at upstream and downstream stations
26-9-2007	148	Decaying lake	Field site visit
7-10-2007	159	Peak discharge of Typhoon Krosa	Streamflow at upstream and downstream stations
23-10-2007	175	Lake disappearance	Simulated
6-1-2008	250	Drained lake bed	Field site visit
22-2-2008	297	Low flow	Field survey

debris flow activity in this tributary, causing the episodic growth and incision of the debris fan at its mouth. One such episode caused the formation of the tributary-dammed lake in August 2007. More recently, an even stronger alluviation event occurred at this location, triggered by the record-setting rainfall brought by Typhoon Morakot, in August 2009. Based on WRA survey data, this event caused 20 m of river bed aggradation 3 km downstream of the Pu-tun-pu-nas confluence. The 2007 lake formation episode thus represents a remarkable, but not exceptional event for this tributary confluence.

[12] River bed changes downstream of the Pu-tun-pu-nas confluence are of engineering concern because of a major water resources scheme that is currently being implemented by the WRA. Called the Tseng-Wen Reservoir Transbasin Diversion Project, the scheme is to divert part of the water discharge of the Laonong River to the Tseng-Wen Reservoir, two valleys away (Figure 2b). The project involves two tunnels pierced through mountain ridges, an aqueduct, and a weir across the Laonong River. The site of this weir, not yet built, is located only 3 km downstream of the Pu-tun-pu-nas confluence (Figure 2c). Tunneling works were under way, and the overall scheme was scheduled for completion before 2012 [*Yang et al.*, 2009]. Delays are likely, however, following the major alluviation event of August 2009, which buried the Laonong tunnel entrance under a thick cover of sediment. In retrospect, the August 2007 lake formation episode can be seen as a precursor event, highlighting the potential of local tributaries to supply massive amounts of sediment to the trunk river.

2.2. Lake Observations

[13] The debris fan at the Pu-tun-pu-nas confluence prior to the damming event is shown in Figure 3a. We observed fan aggradation (Figure 3b) and the presence of a lake upstream of this confluence on 26 September 2007, 1 month after the passage of Typhoon Wutip (8–9 August) and Typhoon Sepat (16–19 August) and a week after Typhoon Wipha (17–19 September). At that time, the trunk river had already reincised the fan by several meters, but the lake had not yet drained (Figure 3c). The lake drowned the trunk river upstream of the confluence over a length of approximately 800 m. We revisited the site on 6 January 2008, 3 months after the passage of Typhoon Krosa (4–7 October), the last typhoon of 2007 (Figure 3d). By this time, the lake was entirely eliminated, and the reincision of the fan by the trunk river had left a 20 m high terrace riser bounding the abandoned fan. Upstream of this newly formed fan terrace, a flight of fluvial terraces up to 8 m in height was observed along the trunk river. These terraces are widely capped by 1–2 m thick sands, interpreted to have accumulated along sheltered sides of the flood channels during the episode.

[14] The lake formation episode caused the destruction of the Hsing-huei Bridge, built across the Laonong River 1 km upstream of the Pu-tun-pu-nas confluence (Figure 2c). Constructed in 1995, this road bridge had a span of approximately 100 m. On 26 September 2007, we observed that the bridge deck had been swept away, leaving its abutments and central pile intact (Figures 3e and 3f). The deck failure appears to have involved buoyant uplift and horizontal drag by flood waters, similar to the failure mode of various coastal bridges destroyed by Hurricane Katrina [*Chen et al.*, 2009]. In 2005, the WRA instrumented Hsing-huei Bridge with an automated stage measurement device. This stopped operating on 19 August 2007, after recording a rapid water rise up to the level of the bridge deck [*Water Resources Agency*, 2007]. We believe that this rise in level ensued from the growth of the tributary-dammed lake. The timing of the bridge destruction thus indicates that it is mainly typhoons Wutip and Sepat, rather than Typhoon Wipha, which caused the aggradation of the Pu-tun-pu-nas debris fan and the resultant lake formation.

[15] Except for incision and trimming by both the trunk and tributary channels, we do not observe significant changes in topography of the Pu-tun-pu-nas debris fan from 26 September 2007 to 6 January 2008 (Figure 4). This implies that the amount of sediment supplied by the Pu-tun-pu-nas River during Typhoon Krosa was relatively small, compared to that supplied during typhoons Wutip and Sepat. Still, flood waters generated during Typhoon Krosa were high enough to undermine the abutment of a 12 year old suspension bridge located 2 km upstream of the Pu-tun-pu-nas River junction. To facilitate reference, the key dates mentioned in our account of the river and lake evolution are listed in Table 1.

3. Data Collection and Analysis

3.1. Topographic Survey Data

[16] Topographic surveys of the river bed were performed both before and after the 2007 episode of lake formation and decay (Figure 5). The first survey was performed by the

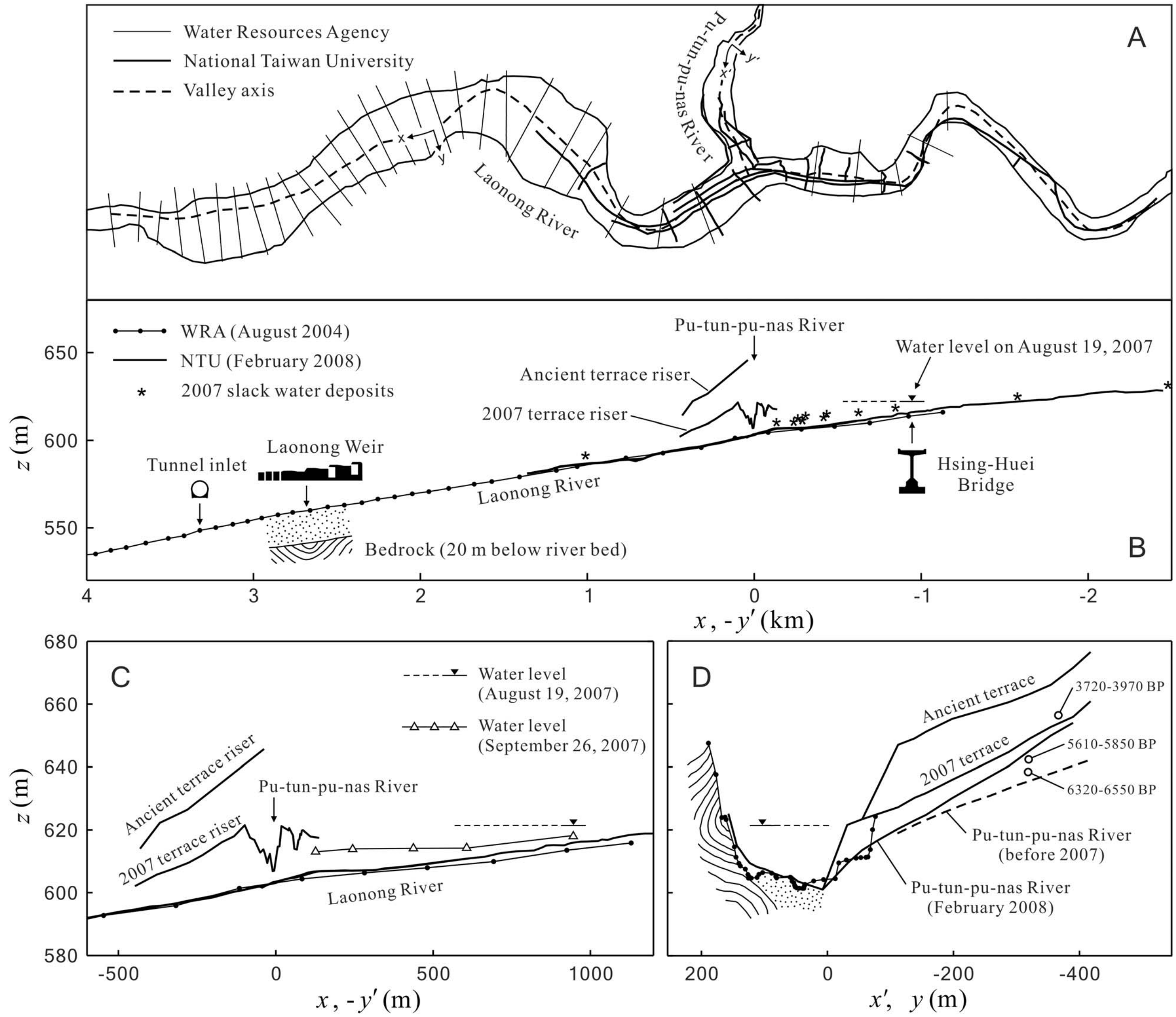

Figure 5. Topographic data surveyed before and after the 2007 episode of lake formation and decay. (a) Plan view of the survey lines; (b) long profiles of the trunk river, tributary terrace riser, and slack-water deposits; (c) close-up of the lake site with reconstructed water levels; and (d) cross section of the trunk river and tributary long profile at the confluence. Wood samples retrieved from the exposed flank of the elevated fan terrace indicate ages ranging from 6500 to 1400 years before present [from *Hsieh and Chyi*, 2010]. Similar in geometry to the new terrace created in 2007, this ancient terrace may be the remnant of a large tributary dam. The left bank of the trunk river opposite the tributary is composed of exposed bedrock.

WRA in August 2004, 1 month after Typhoon Mindulle (28 June to 3 July). The WRA survey covers the trunk river only, from 1 km upstream to 5 km downstream of the confluence, and includes 51 regularly spaced cross sections. We performed the second survey in February 2008, during the low flow period. This survey includes long profiles of the water line and the tributary terrace riser, supplemented by 12 cross sections of the trunk river and the tributary fan. Along the sheltered sides of the Laonong River, some cross sections feature thick sand-capped bars, which we interpret as slack-water deposits [*Jones et al.*, 2001; *Bohorquez and Darby*, 2008]. Their elevations are taken as indicators of the water stage reached during the high flow preceding our survey (Typhoon Krosa flood). To enable retrieval of elevation data from past photographs, we further surveyed recognizable feature points that could serve as controls for photograph calibration. We used this approach to retrieve water surface data from 5 ground photographs acquired on 26 September 2007, when the lake was still present.

[17] The results of our survey are linked to those of the WRA through a common benchmark. This was installed in July 2004 by the WRA on the right abutment of Hsing-huei Bridge, and, fortunately, was not washed away by the flood. To convert survey data to long and transverse profiles, we constructed a system of valley axes and transects, following the approach of *Capart et al.* [2007a]. We use this system to define along valley and across valley coordinates (x, y) for the Laonong River, and (x', y') for the Pu-tun-pu-nas

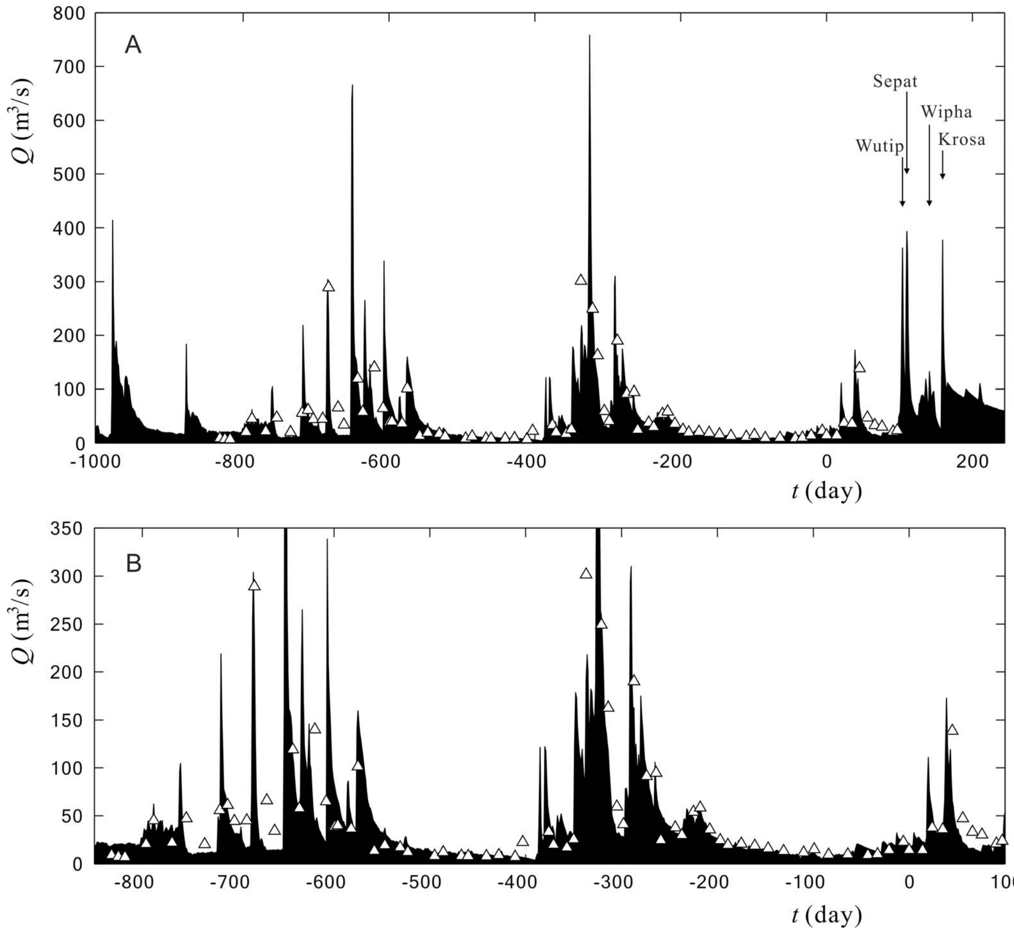

Figure 6. Streamflow at Hsing-huei Bridge from August 2004 to December 2007. (a) Full hydrograph and (b) close-up of the range over which the measured and estimated discharges can be compared. Black silhouette, daily streamflow estimated by averaging signals from upstream and downstream stations. Exceptions are March–September 2005 (only the upstream signal is used), and October 2005 to May 2006 (only the downstream signal is used). Triangles, discharge measurements at Hsing-huei Bridge. Peak labels are typhoon names, and time $t_0 = 0$ corresponds to the beginning of the 2007 typhoon season (1 May 2007).

tributary, with a common origin positioned at the confluence (Figure 5a).

3.2. Streamflow Data

[18] The Laonong River discharge is recorded at two gauging stations of the WRA: Laonong Station (station 1730H031), located 24 km downstream of Hsing-huei Bridge, and Achiba Bridge (station 1730H044), located 8 km upstream. A continuous stage record is available at Hsing-huei Bridge from 1 January 2005 to 19 August 2007. Direct measurements of discharge were also conducted 2 or 3 times per month at Hsing-huei Bridge, until the bridge was destroyed (Figure 6).

[19] Because of river bed aggradation and degradation, discharge measurements at Hsing-huei Bridge show no clear relation with simultaneous stage measurements at the same site (Figure 7a). Even for the period covered by the data, it is therefore not feasible to estimate the daily flow rate at Hsing-huei Bridge from the measured daily stage data. The discharge at the bridge, however, correlates well with simultaneous discharge records at Laonong Station and Achiba Bridge. A daily streamflow signal at Hsing-huei Bridge can thus be derived from these records, considering that discharge at a site is proportional to its contributing watershed area. This yields two estimates,

$$Q_1(t) \approx \frac{A}{A_u} Q_u(t), \; Q_2(t) \approx \frac{A}{A_d} Q_d(t). \tag{1}$$

Here $Q_u(t)$ is the daily discharge at the upstream station (contributing area $A_u = 404$ km^2), $Q_d(t)$ is the daily discharge at the downstream station (contributing area $A_d = 812$ km^2), and $A = 542$ km^2 is the contributing area at Hsing-huei Bridge. In practice, we average $Q_1(t)$ and $Q_2(t)$, except for two periods during which data from one of the two stations are inconsistent with the partial measurements at Hsing-huei Bridge. The resulting reconstructed daily streamflow record is plotted in Figure 6, together with the discharge measurements at the bridge. The estimated and measured flow rates generally agree, and the reconstruction allows us to extend

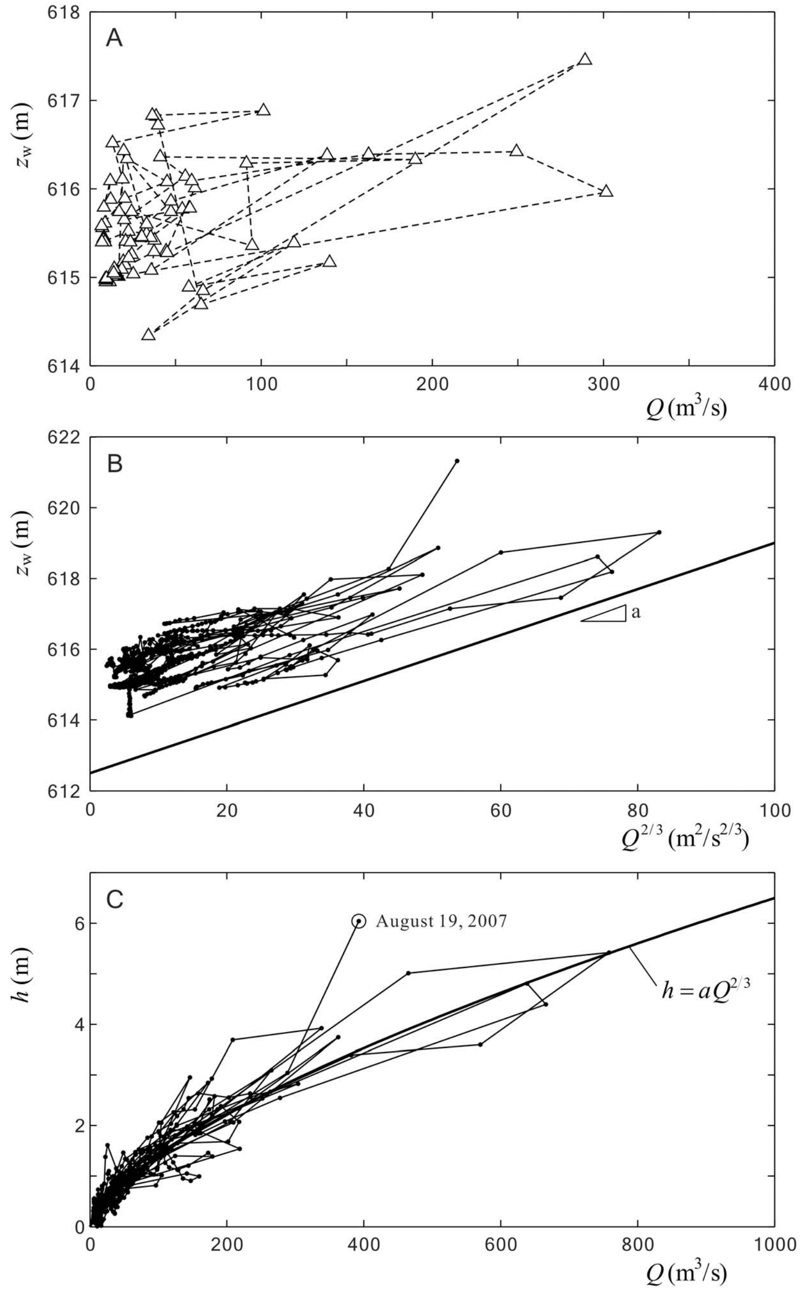

Figure 7. Variation of stage and depth with discharge. (a) Absence of a one-to-one relation between measurements of stage and discharge at Hsing-huei Bridge. (b) Relation between measured stage z_w and estimated daily discharge Q at Hsing-huei Bridge (on a plot of z_w versus $Q^{2/3}$ the short term variations trace parallel segments of approximately constant slope a). (c) Reconstructed depth-discharge relation.

the discharge record at Hsing-huei Bridge to periods of no direct measurements.

3.3. Stage-Discharge Relation at Hsing-huei Bridge

[20] The reconstructed daily streamflow at Hsing-huei Bridge can be used to re-examine the relation between stage and discharge at that location. In Figure 7b, we plot the measured stage record at the bridge against the discharge estimated by equation (1), raised to the power 2/3. Like the partial data of Figure 7a, the daily data of Figure 7b do not fall on a single rating curve. Short term variations, however, trace mutually parallel curve segments consistent with the law of parallelism of ratings [*Freeman and Bolster*, 1910; see *Schmidt and Yen*, 2008]. These segments conform to the relation

$$z_w = aQ^{2/3} + b = aQ^{2/3} + z_s \quad (2)$$

with the same slope $a \approx 0.065$ for all segments, but different offsets b, associated with changes in river sediment bed elevation z_s (assuming a channel reach of approximately constant width). We use this observation to obtain a depth-discharge relationship. Assuming that the sediment bed elevation evolves more slowly than either the discharge or the water stage, we approximate the instantaneous bed elevation at a given day t by its average over the previous week,

$$\bar{z}_s(t) = \frac{1}{7}\int_{t-8}^{t-1}\left(z_w - aQ^{2/3}\right)dt, \tag{3}$$

where time is expressed in days. The interval of 1 week is chosen to resolve bed elevation changes, while filtering out daily stage variations due to changes in discharge. We can then estimate the water depth on day t from

$$h(t) = z_w(t) - \bar{z}_s(t), \tag{4}$$

constructed without using the discharge $Q(t)$ on day t. Figure 7c shows the depth-discharge relation obtained in this way, plotting the depth $h(t)$ estimated from equations (3) and (4) against the daily discharge $Q(t)$ from equation (1). As expected, the data points approximately collapse onto a rating curve of the assumed form. This confirms that the water level at Hsing-huei Bridge generally rises and falls under the influence of two contributions; that is, fast variations due to transient streamflow $Q(t)$, and slow variations due to changes in local sediment bed elevation $z_s(t)$. The plot also highlights an exception to this rule, on the last day of data acquisition prior to the submersion of Hsing-huei Bridge. On 19 August 2007, the water level attained a record high, reaching the bridge deck, in a way that cannot be accounted for by the rating curve. On its own, the flow rate $Q(t)$ on that day was not sufficient to raise the water depth so high. Instead, the bridge was likely submerged by the backwater profile associated with the aggrading tributary dam, 1 km downstream. This is consistent with the maximum elevation of the tributary dam crest, as inferred from the longitudinal terrace riser profile (Figure 5c) and the transverse fan terrace profile (Figure 5d).

4. Mathematical Theory

4.1. Assumptions and Governing Equations

[21] Our aim is to predict the evolution of the long profile of a trunk river subject to strong sediment influx from a tributary. Let $z_s(x, t)$ denote the elevation of the trunk river above a reference datum. The river at time t_0 is taken to start from a known sediment bed profile $z_s(x, t_0)$, where x is the curvilinear coordinate measured along the valley axis in the direction of river flow. For simplicity, we place the origin $x = 0$ at the tributary confluence. We neglect the water flux discharged from the tributary and consider only its sediment contribution, $I(t)$; that is, the volumetric flux of bed material (sediment + pore space) dumped into the trunk river. Here and throughout the theory, we assume that the trunk river flows in a channel of rectangular cross section and constant width B. Under these conditions, the equation governing the evolution of the sediment bed profile $z_s(x, t)$ is the Exner equation [see *Paola and Voller*, 2005]

$$B\frac{\partial z_s}{\partial t} + \frac{\partial J}{\partial x} = I(t)\delta(x), \tag{5}$$

where $J(x, t)$ is the bed load transport rate in the trunk river, defined as a flux of bed material volume (sediment + pore space) across a given cross section. The Dirac delta $\delta(x)$ on the right-hand side of the equation is used to represent the tributary sediment influx as a point source of time-varying strength $I(t)$ at the origin.

[22] In addition to the sediment bed profile $z_s(x, t)$, we also simulate the water surface profile $z_w(x, t)$ along the trunk river. We assume that the unsteady water discharge $Q(t)$ varies sufficiently slowly that it can be considered uniform along the valley segment of interest. Accordingly, the water surface is taken to adjust in a quasi-steady manner to the evolution of the sediment bed. Following *Hsu and Capart* [2008], we subdivide the river reaches into two types: Running-water reaches, where uniform flow parallel to the sediment bed is assumed; and standing-water reaches, where an approximately horizontal backwater profile is forced from downstream. At each location x, the water surface must satisfy the following system of complementary inequalities:

$$z_w - z_s \geq h_0,\ \frac{\partial z_w}{\partial x} \leq 0,\ (z_w - z_s - h_0)\frac{\partial z_w}{\partial x} = 0, \tag{6}$$

where h_0 is the normal depth of the flow in reaches of running water. In the above system, the first inequality states that the water depth $z_w - z_s$ must either coincide with (in running-water reaches) or exceed the normal depth (in standing-water reaches). The second inequality requires the water surface to either tilt down-valley (in running-water reaches) or approach the horizontal (in standing-water reaches). The last condition holds that at any location x, one or the other of the inequalities must reduce to an equality, insuring that the reach is characterized by either running or standing water. Running and standing water reaches represent simplifications of the standard hydraulic profiles into reaches of uniform flow and horizontal stage, respectively. A gradually varying profile M1, for instance, is simplified into its upstream (bed-parallel) and downstream (horizontal) asymptotes. The third relation is the switch criterion that allows a rising lake profile (standing water) to gradually drown an upstream uniform flow reach (running water). It also controls the transition from standing water to running water at a lake outlet, allowing lake drainage to occur. Taken as a whole, the system forces the water surface to decrease monotonously from upstream to downstream, even if the sediment bed profile does not. Because the sediment bed $z_s(x, t)$ evolves in time, the subdivision between running-water and standing-water reaches is not fixed, but continuously adjusts to the topography.

[23] To simplify matters further, we assume that the normal depth $h_0(x, t)$ depends only on the instantaneous discharge $Q(t)$, as specified by the depth-discharge relation

$$h_0(x, t) = h_0(Q(t)) = \left(\frac{Q(t)}{CBg^{1/2}}\right)^{2/3}, \tag{7}$$

where C is a dimensionless rating curve coefficient assumed constant along the valley segment considered, B is the width, assumed constant, and g is gravitational acceleration. With the equivalence $a = (CBg^{1/2})^{-2/3}$, this is simply a dimensionally consistent version of the empirical depth-discharge relation of equation (2). The above description may appear a drastic oversimplification of the standard theory of open-channel flow [see e.g., *Henderson*, 1966]. In sections 4.2

and 4.3, however, we will show that the resulting predictions agree well with both experimental and field data.

[24] We finally link the bed load transport rate $J(x, t)$ to the prevailing river bed and flow conditions. Following *Hsu and Capart* [2008], we adopt the following modified stream power law for bed load transport:

$$J(x,t) = KQ(t)\max\left\{-\frac{\partial z_w}{\partial x} - S_{\min}, 0\right\}, \qquad (8)$$

where K is a dimensionless transport coefficient, and $S_{\min}$ is the slope threshold proposed by *Mitchell* [2006; see also *Lai and Capart*, 2007], below which transport is taken not to occur. In the above relation, the gradient term driving sediment transport is provided by the water surface slope $-\partial z_w/\partial x$, not the sediment bed slope $-\partial z_s/\partial x$. This choice is made in order to suppress bed load transport in reaches of standing water, where $\partial z_w/\partial x = 0$. When the slope threshold is set to zero ($S_{\min} = 0$), and where $S = -\partial z_s/\partial x = -\partial z_w/\partial x$ (in reaches of running water), the relation reduces to the classical stream power relation $J \propto QS$ proposed by *Lane* [1955]. When only reaches of running water are present (even when $S_{\min} \neq 0$), substitution of the above transport relation into the Exner equation (equation (5)) yields the linear diffusion equation with source term,

$$B\frac{\partial z_s}{\partial t} - KQ(t)\frac{\partial^2 z_s}{\partial x^2} = I(t)\delta(x), \qquad (9)$$

with a time-varying diffusivity $D(t) = KQ(t)/B$. In contrast with the assumptions in *Hsu and Capart* [2007], here both the tributary input I and stream discharge Q are allowed to vary with time. When reaches of standing water are present, transport is locally suppressed, making the diffusivity nonuniform and the problem nonlinear. For steady water discharge without tributary influx, equation (9) further reduces to the linear diffusion theory of alluvial profile evolution [see *De Vries*, 1973; *Soni et al.*, 1980; *Begin et al.*, 1981; *Jain*, 1981; *Ribberink and Van der Sande*, 1985].

[25] Note that both the diffusional approach and our running/standing water approximation apply only over the reach scale. Disregarded are, for instance, the details of how a water profile M1 is needed to smoothly connect a uniform flow reach with a horizontal lake surface. Moreover, the validity of both approximations is expected to depend on channel steepness. For channels of milder slope, longer length and time scales would be required for the approximation to become valid. For the upper Mississippi River upstream and downstream of Lake Pepin, for instance [*Schumm*, 2005; *Hsu and Capart*, 2008; *Blumentritt et al.*, 2009], length scales of the order of 10 km would be needed, as compared to length scales of the order of 100 m for the much steeper Laonong River. For evolving river long profiles in the absence of lakes, the validity of the local uniform flow assumption was recently analyzed in detail by *Fasolato et al.* [2010].

[26] In summary, the above theory requires information about the valley segment to set the channel width B, the initial conditions $z_s(x, t_0)$ and boundary conditions upstream and downstream. River discharge $Q(t)$ and tributary sediment supply $I(t)$ must also be prescribed. Finally, one must select appropriate values for the following dimensionless constitutive coefficients: K (bed load transport coefficient), $S_{\min}$ (bed load transport slope threshold), and C (depth-discharge rating curve coefficient). These coefficients can either be calculated on the basis of more detailed descriptions of water flow and sediment transport, or calibrated from available experimental or field data. In what follows, we will adopt the second approach and check that the above data requirements can be met, even for a field case where only partial information is available.

4.2. Numerical Scheme

[27] Under the special circumstances of uniform initial slope and constant rates of water and sediment influx, it was shown in *Hsu and Capart* [2008] that the above equations admit self-similar analytical solutions. In particular, such solutions can describe the growth of a tributary-dammed lake under conditions of strong constant sediment influx. In the present study, however, we are interested in more general conditions for which analytical solutions are insufficient. To describe the full life cycle of a tributary-dammed lake, we must construct solutions by numerical means. For this purpose, we set up the following finite volume discretization. A finite domain $x_U \le x \le x_D$ is assumed, with upstream and downstream boundaries x_U, x_D, inside which the sediment bed and water surface elevations $z_s(x_i)$, $z_w(x_i)$ are sampled at equally spaced positions

$$x_i = x_U + \left(i - \frac{1}{2}\right)\Delta x, \qquad (10)$$

where $i = 1,\ldots, m$ and $\Delta x = (x_D - x_U)/m$. At any given time t, the water surface profile $z_w(x, t)$ can be found from the sediment bed profile $z_s(x, t)$ using the solution

$$z_w(x,t) = \max_{\xi \ge x}\{z_s(\xi, t)\} + h_0(Q(t)), \qquad (11)$$

constructed to satisfy the complementary inequalities of equation (6). For a discrete profile $z_s(x_i)$, this translates into the following very simple algorithm. Assuming a given water level $z_w(x_m)$ at the last grid point, the full water profile $z_w(x_i)$ is obtained by iterating the statement

$$z_w(x_i) = \max\{z_w(x_{i+1}), z_s(x_i) + h_0\}, \quad i = m-1, m-2, \ldots, 1, \qquad (12)$$

which represents a one-way sweep from downstream to upstream. Once the water surface profile is known, the sediment bed profile at the next time step can be obtained by integrating the Exner equation (equation (5)). The sediment bed level $z_s(x_i)$ is advanced from time t_k to time $t_{k+1} = t_k + \Delta t$ using the explicit finite volume statement

$$z_s(x_i, t_{k+1}) = z_s(x_i, t_k) + \frac{\Delta t}{B\Delta x}\{J_{i-1/2} - J_{i+1/2}\} + \frac{\Delta t}{B\Delta x}I_i. \qquad (13)$$

The second term on the right represents the balance of bed load fluxes across the upstream and downstream faces of each finite volume. These bed load fluxes $J_{i+1/2}$ are calculated using the following discrete version of the modified stream power law (equation (8))

$$J_{i+1/2} = KQ\max\left\{-\frac{z_w(x_{i+1}) - z_w(x_i)}{\Delta x} - S_{\min}\,,\ 0\right\}, \qquad (14)$$

Table 2. Simulation Input and Output Parameters[a]

Category	Parameter / Symbol	Laboratory Run	Field Event
Trunk river channel	Width B	10 mm	90 m
Trunk river initial conditions at time $t_0 = 0$	Confluence elevation z_0	0 m	603.75 m
	Upstream slope S_U	0.11	0.0115
	Downstream slope S_D	0.11	0.0175
Trunk river normal depth and bed load transport relation	Normal depth h_0	2 mm	n.a.
	Rating curve coefficient C	n.a.	0.21
	Slope threshold S_{min}	0.077	0
	Transport coefficient K	1.66	0.040
Tributary sediment influx	Influx intensity $\kappa = I_1/Q$	0.242	0.0025
	Influx starting time t_1	0	99 d
	Influx stopping time t_2	239 s	137 d
Tributary-dammed lake response	Maximum dam elevation z_s^{max}	54 mm	624.5 m
	Maximum lake length L_{max}	38 cm	1625 m
	Time of lake disappearance t_3	379 s	175 d

[a]n.a., not applicable.

where all variables are sampled at time t_k. The third term on the right of equation (13) is the contribution from the tributary sediment influx, given by

$$I_i = \begin{cases} I(t_k), & \text{if } x_i - \Delta x/2 \le 0 < x_i + \Delta x/2, \\ 0, & \text{otherwise.} \end{cases} \tag{15}$$

Note the mass conservation property of the finite volume statement (equation (13)). If the tributary source term is turned off ($I(t) = 0$) and no sediment enters through the domain boundaries, sediment can be transferred between cells but the total sediment volume $\sum_i z_s(x_i) B \Delta x$ will not vary. Because the rate-setting process is a diffusion equation, with diffusivity $D = KQ/B$, the stability of the explicit scheme is subject to the condition

$$\Delta t < \frac{1}{2}\frac{(\Delta x)^2}{D}. \tag{16}$$

For the calculations presented below, we start from piecewise linear initial conditions

$$z_s(x, t_0) = \begin{cases} z_0 - S_U x, & x_U < x \le 0, \\ z_0 - S_D x, & 0 \le x < x_D, \end{cases} \tag{17}$$

where S_U and S_D are upstream and downstream initial slopes. We further send the boundaries x_U and x_D sufficiently far upstream and downstream of the valley segment of interest to be able to assume the following running water, constant flux conditions at the boundaries:

$$J_{1/2} = J(x_U) = KQ \max\{S_U - S_{min}, 0\}, \tag{18}$$

$$J_{m+1/2} = J(x_D) = KQ \max\{S_D - S_{min}, 0\}, \tag{19}$$

$$z_w(x_m, t_k) = z_s(x_m, t_k) + h_0(Q(t_k)). \tag{20}$$

With these initial and boundary conditions, the numerical scheme is now completely specified. A calculation example is presented next.

4.3. Calculation Example

[28] To illustrate the theoretical and numerical description, we consider the following conditions, corresponding to one of the experimental runs of *Hsu* [2007]. The narrow channel of width $B = 1$ cm starts from an alluvial bed of constant inclination $S_U = S_D = S_0 = 0.11$, in equilibrium with the water discharge $Q = 4.67$ mL s^{-1} and background sediment flux $J_0 = 0.256$ cm^3 s^{-1} supplied upstream of the channel, both held steady throughout. The tributary sediment influx follows the simple history

$$I(t) = \begin{cases} 0, & t < t_1, \\ I_1, & t_1 \le t < t_2, \\ 0, & t_2 \le t. \end{cases} \tag{21}$$

[29] The influx at location $x = 0$ is started at time $t_1 = 0$ s, held constant at value $I_1 = 1.13$ cm^3 s^{-1} over time interval $t_1 \le t < t_2$, and terminated at time $t_2 = 239$ s. Because the water discharge is held steady in this case, a single value $h_0 = 2$ mm is adopted for the normal flow depth, corresponding to the experimentally observed water depth over the initial constant slope bed. Separate measurements of bed load transport J in steady uniform flow for various discharges Q and channel slopes $S = -\partial z_s/\partial x = -\partial z_w/\partial x$ were performed by *Hsu* [2007] to characterize the bed load transport relationship $J(Q, S)$ for the conditions of her experiments. These data were used to determine best fit values $K = 1.66$ and $S_{min} = 0.077$ for the transport coefficients (see Table 2 for a summary of input and output parameters). Numerical computations are performed with upstream and downstream boundaries at locations $x_U = -200$ cm, $x_D = 200$ cm, spatial step 5 mm, and time step $\Delta t = 0.01$ s. We checked our choice of space and time steps by verifying that the root-mean-square error between numerical and analytical bed profiles, calculated over range $|x| \le 1000$ mm, is inferior to 0.1 mm at the time of maximum dam growth. Compared to the maximum dam height, this amounts to a relative error smaller than 0.2%.

[30] Computed results are presented in Figure 8. The first panel (Figure 8a) shows the evolution of the channel during the period $t_1 \le t < t_2$ when the tributary sediment flux is active. The corresponding strong sediment influx at the origin $x = 0$ forces the formation and growth of a tributary-dammed lake. Fed by the tributary, aggradation of the main channel occurs downstream of the tributary junction, creating a deposit of maximum thickness at the junction itself. This generates a dam crest of rising elevation, upstream of which ponds a lake of rising stage and expanding length. The upstream transgression of the lake gradually drowns

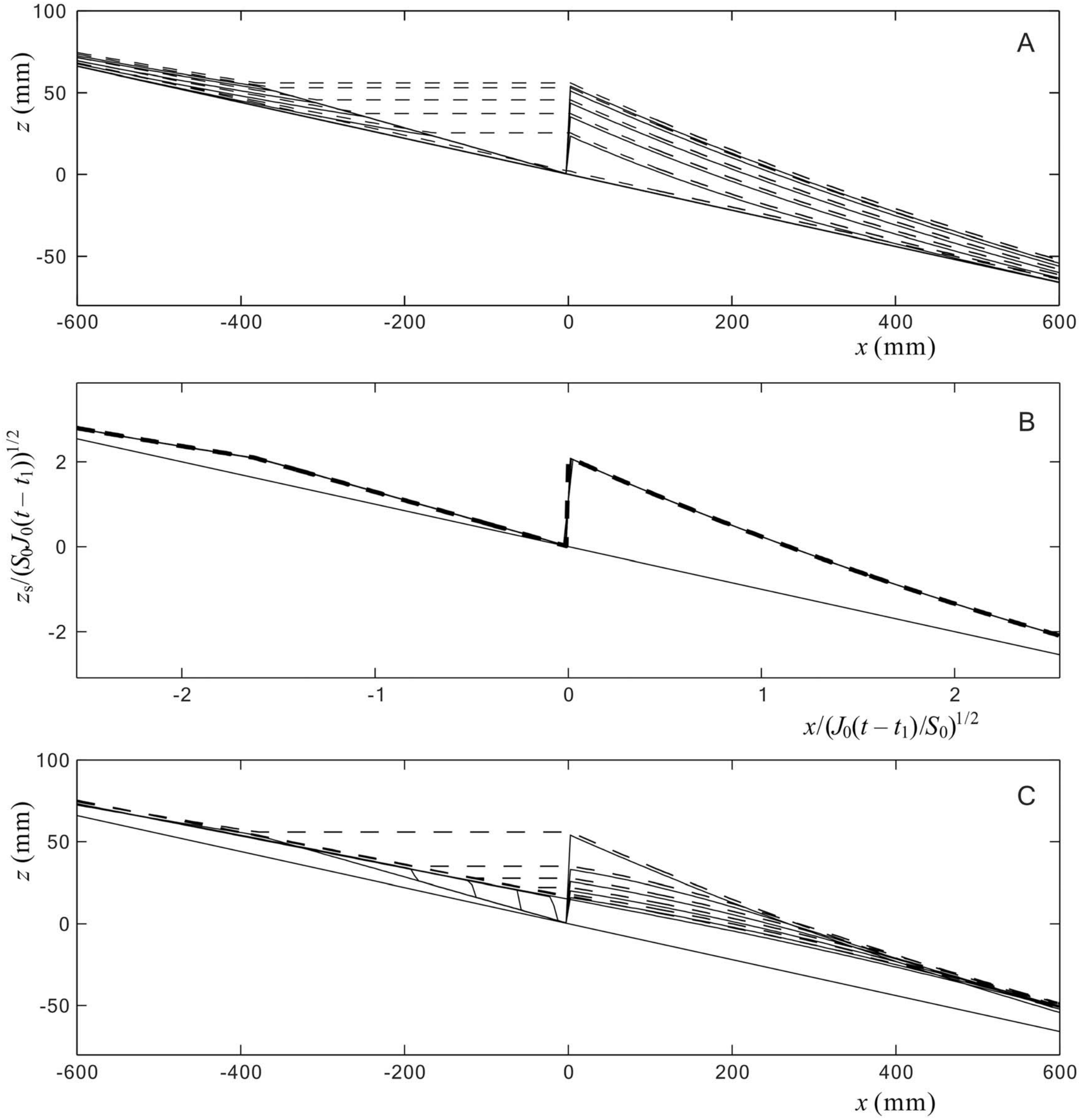

Figure 8. Predicted profiles for laboratory example of lake growth and decay. (a) Computed stream bed (solid lines) and water stage profiles (dashed lines) at times t = 0, 46, 103, 157, 214, and 239 s (lake growth); (b) comparison of the calculated stream bed profiles of Figure 8a (thin solid lines) with the analytical solution of *Hsu and Capart* [2008] (bold dashes), in normalized coordinates highlighting self-similarity; and (c) computed stream bed (solid lines) and stage profiles (dashed lines) at times t = 239, 268, 298, 332, 365, and 393 s (lake decay and elimination), with the initial stream bed profile (t = 0) added for reference. Flow here and in Figures 9, 10, 11, and 14 is from left to right.

thin deposits laid down by the upstream river. Over this evolving sediment bed profile, the water surface is parallel to the bed profile upstream and downstream of the lake, corresponding to reaches of running water, and horizontal in the zone of standing water associated with the lake, where sediment transport is suppressed. Because the dam aggradation is gradual, the water flow across the lake and past the dam crest is never interrupted, and the formation of the lake blocks sediment transit only.

[31] For the period of dam and lake growth covered by Figure 8a, neither the initial conditions (a linear profile) nor the sediment influx (a point source at the origin) impose any externally prescribed length scale on the problem. This allows the sediment bed profile to respond in the geometrically self-similar fashion

$$\frac{z_s}{\sqrt{S_0 J_0 (t-t_1)}} = f\left(\frac{x}{\sqrt{J_0(t-t_1)/S_0}}\right). \tag{22}$$

In *Hsu and Capart* [2008], we exploited this special characteristic to derive the similarity function $f(\cdot)$ in ana-

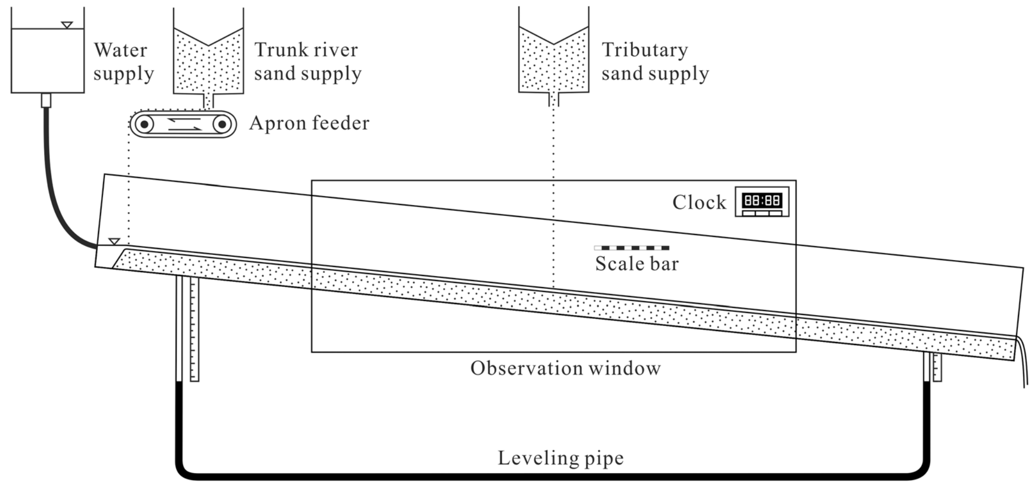

Figure 9. Laboratory setup used for the experiments of *Hsu* [2007].

lytical form. This function is defined piecewise by the following expressions

$$f(\xi) = \begin{cases} -\xi + \dfrac{2\mu}{\mathrm{erfc}\left(\frac{1}{2}\lambda\right)}\,\mathrm{ierfc}\left(-\frac{1}{2}\mu\xi\right), & \xi \le -\lambda/\mu, \\ -2(I_1/J_0 - 1)\mu^2\xi/(\sqrt{\pi}\lambda), & -\lambda/\mu \le \xi < 0, \\ -\xi + 2(I_1/J_0 - 1)\mu\,\mathrm{ierfc}\left(\frac{1}{2}\mu\xi\right), & 0 \le \xi, \end{cases} \tag{23}$$

where $\mu = \sqrt{1 - S_{\min}/S_0}$, and function $\mathrm{ierfc}(\xi) = \exp(-\xi^2)/\sqrt{\pi} - \xi\,\mathrm{erfc}(\xi)$ is the first integral of the complementary error function $\mathrm{erfc}(\xi) = 1 - \mathrm{erf}(\xi)$ [see *Carslaw and Jaeger*, 1959]. The parameter λ is the root of a transcendental equation taking numerical value $\lambda = 0.893$ for the conditions of this particular run ($S_{\min}/S_0 = 0.7$, $I_1/J_0 = 4.4$). To check the numerical scheme, computed profiles are compared with the analytical solution in Figure 8b. Excellent agreement is recorded: Plotted in normalized coordinates, the numerical sediment bed profiles obtained for different times $t = 0$ to 239 s very nearly coincide, collapsing onto the analytical curve of equation (23).

[32] Because lake decay starts from generic conditions, inherited from the tributary-damming process, the analytical solutions derived by *Capart et al.* [2007b] for lake breaching and infill do not apply. Numerical computations can proceed, however, and the resulting profiles are shown in Figure 8c. They cover the period $t_2 \le t \le t_3$ between the termination of the tributary sediment supply and the complete elimination of the lake. Upon termination of the sediment supply, at time $t_2 = 239$ s, the lake decays due to two simultaneous processes. Downstream, degradation of the river bed occurs, leading to the gradual erosion of the lake outlet and associated drainage of the lake. Upstream, delta progradation into the shrinking lake leads to infill of the lake depression. The lake is eliminated when the combined infill and erosion shrink the lake to a point. After upstream and downstream reaches merge back together, the reconnected alluvial channel continues to evolve under the action of running water. The time t_3 at which the lake disappears is not prescribed by the external conditions, but computed as part of the solution. In this particular case, the value obtained for the time of lake elimination is $t_3 = 379$ s. Qualitatively, the lake formation and decay processes presented in Figure 8 agree with descriptions by *Lane* [1955] and *Holmes* [1945; pp. 155–156 and Figure 66]. Quantitative comparisons with laboratory and field profiles are presented in sections 5 and 6.

5. Comparison With Experiments

[33] To test the theory and computations, we first compare calculated results with the laboratory experiments of *Hsu* [2007]. These experiments were used by *Hsu and Capart* [2008] to validate analytical results for lake onset and growth. Here we use them to validate more general numerical solutions for both the growth and decay of a tributary-dammed lake. The experiments were conducted using the setup shown in Figure 9. A long, narrow flume (length = 250 cm, width = 1 cm) is inclined at slope $S_0 = 0.11$ (determined using a leveling tube). Upstream, the flume is supplied with a steady water discharge from a constant head tank, and with a steady flux of sediment from a silo of dry sand. To facilitate control of the sediment flux, the sand does not freely stream down from the bottom outlet of the silo. It is instead entrained laterally by a motor-driven, adjustable speed conveyor belt (apron feeder). Inspired by a similar device at National Central University [*Hsiau et al.*, 2004], this sand-feeding mechanism allows precise fine tuning of the sediment flux simply by varying belt speed. The mechanism is used to adjust the upstream sediment flux to the prescribed slope and water discharge, until equilibrium transport conditions are achieved over a sand deposit of uniform thickness. A second sand silo is used to feed a prescribed influx of dry sand to the middle of the flume. This supply can be activated and deactivated at prescribed times to represent intermittent sediment influx from the tributary. Sand of median diameter $d_{50} = 0.32$ mm and coefficient of uniformity $d_{60}/d_{10} = 1.84$ is used as sediment material. Because of the small flume dimensions,

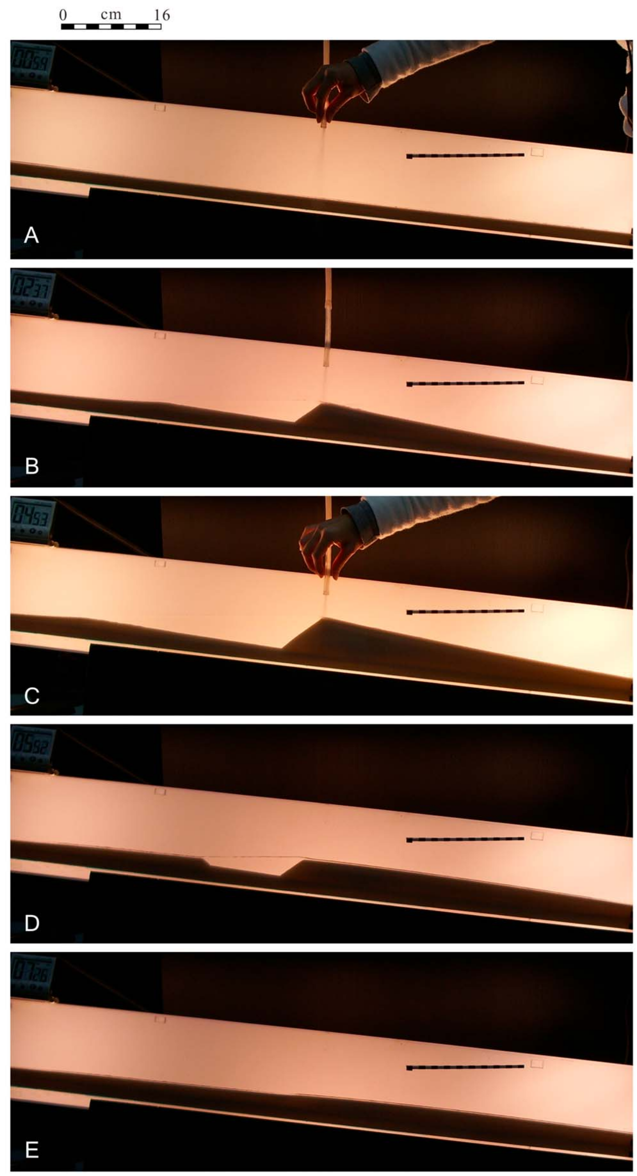

Figure 10. Laboratory example of lake growth and decay, from the experiments of *Hsu* [2007]. (a–e) Photographs at times $t = 0$, 103, 239, 298, and 393 s, respectively. Tributary sediment influx was started at time $t_1 = 0$ (Figure 10a), and stopped at time $t_1 = 239$ s (Figure 10c).

the tests belong to the category of microscale experiments, conducted at such small scales that the flow is laminar or transitional instead of fully turbulent (as in Froude-scale models and actual rivers). *Malverti et al.* [2008] have shown that such experiments can nevertheless be upscaled to turbulent rivers, provided that the focus is on longitudinal river profile evolution.

[34] Selected snapshots for one experimental run are presented in Figure 10. The response of the channel is observed through the transparent side wall of the flume. Lighting is provided by back-illumination through a translucent white panel placed behind the other side wall, and the channel evolution is recorded by time lapse photography. The photographs are used to retrieve sediment bed and water surface profiles at successive times, via a calibrated transformation from image to metric coordinates. The conditions for this run are those adopted earlier for the calculation example (see section 4.3 and Table 2).

[35] The resulting profiles are shown in Figure 11. Overall, the observed response matches that predicted by the theory. For such strong tributary sediment influx ($I_1/J_0 > 2$), a tributary-dammed lake grows during the period of tributary activity $t_1 < t < t_2$, then gradually decays once the tributary sediment influx stops. Lake decay results from two simultaneous processes: Infill by a prograding delta at the lake inlet and erosion of the dam crest at the lake outlet. The lake is eliminated once the prograding delta front reaches the receding dam crest. For this experimental run, the complete elimination of the lake occurs at time $t_3 = 387$ s, which compares well with the predicted time $t_3 = 379$ s obtained from the numerical computations. During degradation, the water discharge was always sufficient to erode the bed over the full flume width, without partial channelization, in agreement with the constant width assumption of the theory.

[36] Despite the overall agreement, minor differences between the simulated (Figure 8) and observed profiles (Figure 11) can be noted. The main discrepancies concern the upstream-facing slope of the tributary dam and the downstream-facing foreset of the prograding delta. Both slopes are assumed vertical in the theory, but relax to the angle of repose of the sediment material ($\phi = 36°$) in the experiments. The influence of this finite angle of repose could be introduced into the theory [*Voller et al.*, 2004; *Lai and Capart*, 2009], but this would complicate the numerical scheme considerably. For this reason, we assume, like *Voller et al.* [2006], that the angle of repose is sufficiently steep relative to the riverbed inclination to be approximated by a vertical (in the analytical solutions) or near-vertical segment (spread over a few grid points in the numerical computations). Also, instead of the sharp dam crests produced in the simulations, more rounded crests are observed in the experiments. This can be attributed to pluviation over a finite width (instead of a point source), and to deviation of the experimental flow from the abrupt transition between horizontal backwater and bed-parallel uniform flow assumed by the theory.

[37] To make the comparison quantitative, we plot in Figure 12 the computed and measured time histories of the bed and water elevation at selected cross sections. For convenience, the experimental values are also listed in Table 3. The bed elevations shown in Figure 12a exhibit distinct responses upstream and downstream of the tributary confluence. At downstream cross sections, the bed evolution tracks the rise and fall of the tributary dam crest, with some delay and attenuation. At upstream cross sections, the bed evolution is more complex due to the influence of the expanding and shrinking lake. Upstream bed elevations within reach of the lake rapidly rise at first, freeze at a constant level when drowned by the lake, then undergo a steplike jump upon passage of the prograding delta associated with lake decay. Cross sections further up valley, never reached by the lake, evolve more gradually under the influence of the wedgelike aggradation upstream of the lake.

[38] Water surface elevations depicted in Figure 12b undergo similar evolutions. Because the channel evolves gradually, the water surface evolution is slaved to the sediment bed evolution, as assumed by the theory. At most

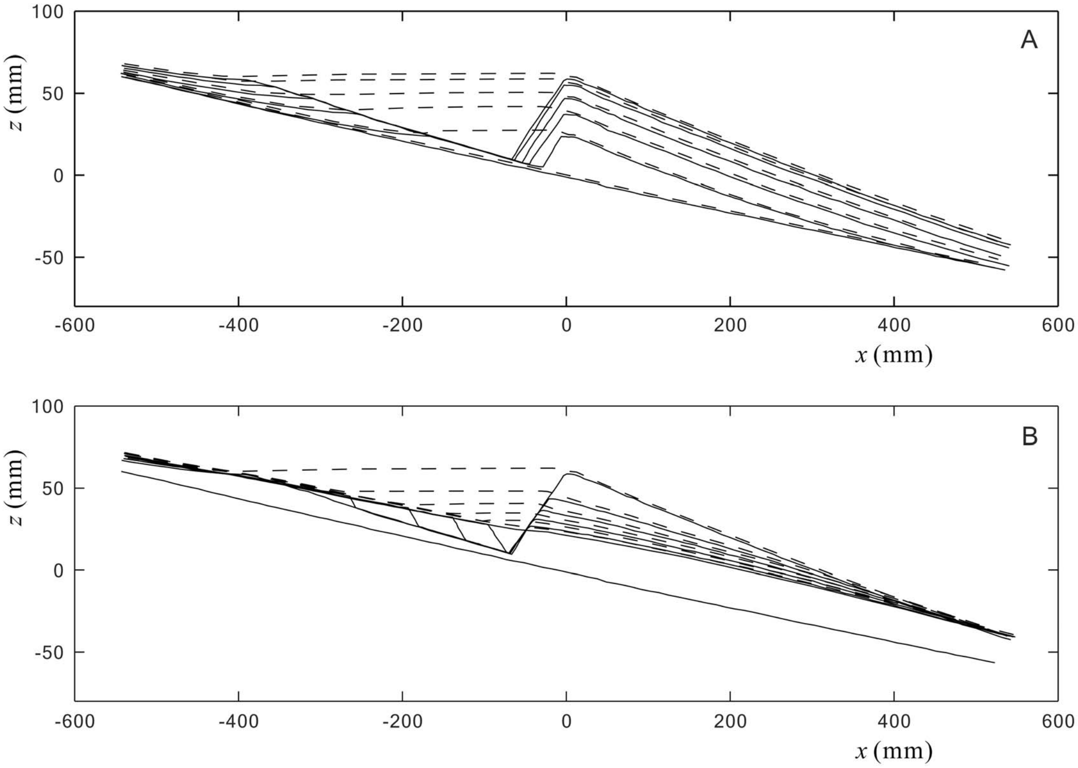

Figure 11. Measured profiles for laboratory example of lake growth and decay. (a) Stream bed (solid lines) and water stage profiles (dashed lines) at times $t = 0$, 46, 103, 157, 214, and 239 s (lake growth). (b) Stream bed (solid lines) and stage profiles (dashed lines) at times $t = 239$, 268, 298, 332, 365, and 393 s (lake decay and elimination) with the initial stream bed profile ($t = 0$) added for reference.

locations, the water stage rises along with the local bed height. The key exception occurs when a cross section is drowned by the lake, in which case nonlocal effects intervene. The water stage is no longer determined by the local bed elevation (increased by the running water depth), but instead rises and falls in lockstep with the water stage at the lake outlet, itself determined by the elevation of the tributary dam crest. For all of the above features, the measured and simulated elevation histories are in good quantitative agreement. Note that the constitutive coefficients of the theory are obtained from separate measurements of the transport relation $J(Q, S)$, not calibrated on the basis of the measured channel response. The level of agreement recorded thus represents a faithful measure of the predictive power of the theory. Adjusting the coefficients based on the measured histories would improve the fit, but would make the comparison less meaningful.

[39] To check that the simulated and measured responses agree over a wider set of conditions than those of a single experimental run, Figure 13 shows lake decay time obtained for 9 different runs (see Table 4 for the measured values). Based on the dimensional analysis outlined in *Hsu and Capart* [2008], the time to lake elimination t_3 should be governed by a relation of the form

$$\frac{t_3 - t_2}{t_2 - t_1} = F\left(\frac{I_1}{J_0}\right), \tag{24}$$

where t_1 and t_2 mark the beginning and end of lake growth, J_0 is the background bed load transport rate in the trunk river, and I_1 is the tributary influx during lake growth. Figure 13 shows the resulting curve, obtained by simulating the full lake life cycle for different ratios I_1/J_0 of tributary sediment influx to trunk river sediment transit. According to the theory [*Hsu and Capart*, 2008], tributary-dammed lakes form only when this ratio exceeds the threshold $I_1/J_0 = 2$. Otherwise, the tributary sediment influx is too weak to force the formation of a lake, and causes instead a cuspate river aggradation. This explains the zero intercept of the calculated curve at $I_1/J_0 = 2$. As seen in Figure 13, the experimental results are in good agreement with the calculations. Again, we stress that this agreement is attained without calibrating simulation parameters against the measured channel responses. For simplified laboratory conditions, the theory and numerical scheme are thus checked to reliably predict the river and lake evolution.

6. Laonong River Simulations

6.1. Parameter Estimation

[40] Using the theory presented in section 4, we now simulate the 2007 episode of lake formation and decay at the confluence of Laonong and Pu-tun-pu-nas rivers. Although we were able to gather much information about this field event (see sections 2 and 3), there remain significant data gaps. Most importantly, the tributary sediment influx hydrograph $I(t)$ is unknown. The model therefore cannot be run simply in forward mode, based on completely known inputs. It must partly be used as an inversion tool, to determine unknown inputs from the available data. For this

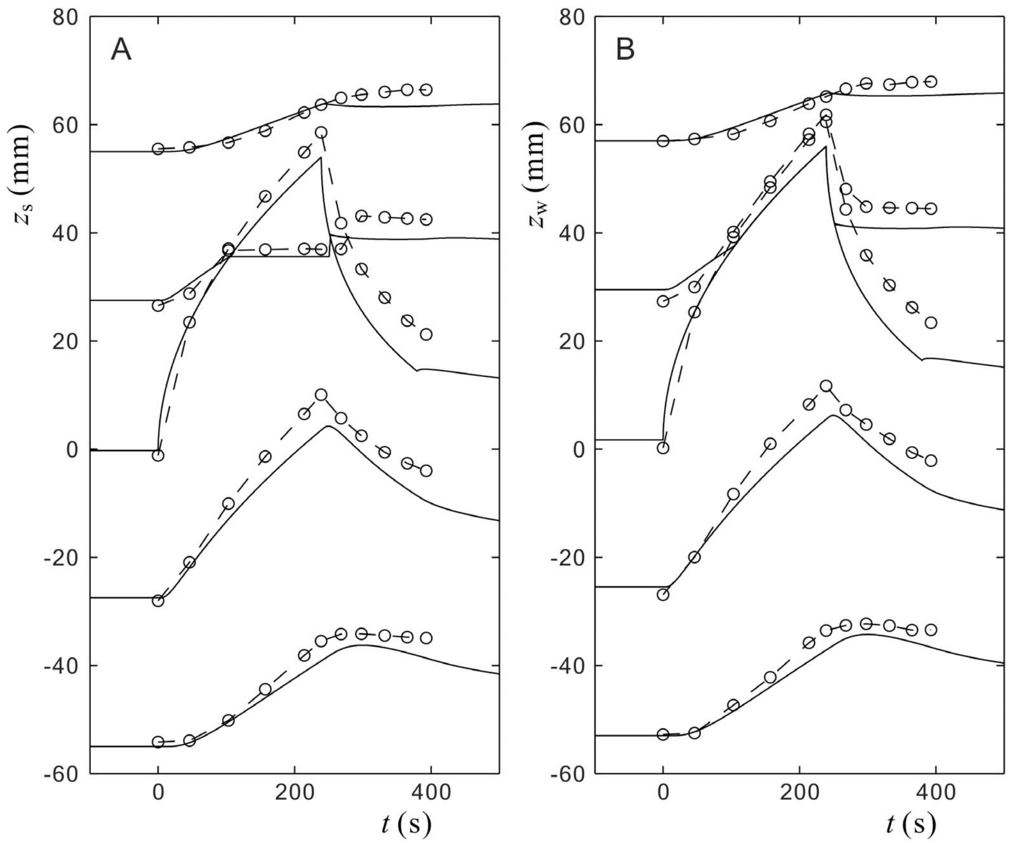

Figure 12. Time evolution of stream bed elevation and water stage for experimental example of lake growth and decay. (a) Predicted (solid lines) and measured (circles connected by dashed lines) bed elevation hydrographs at positions $x = -500$, -250, 0, 250, and 500 mm. (b) Predicted and measured water stage hydrographs at the same positions as in Figure 12a.

purpose, our approach is to reduce the unknowns to a minimal set of parameters, then adjust their values by trial and error to match model outputs with survey data.

[41] Three categories of inputs are needed to model the trunk river response: Choice of initial conditions prior to lake formation; information on the river flow and its bed load transport capacity; and information on the sediment influx from the Pu-tun-pu-nas tributary. In the years preceding the lake event, ground photographs indicate moderate, intermittent sediment supply from the tributary. This was sufficient to maintain a cusped slope break $S_D > S_U$ of the trunk river at the tributary junction, but not enough to force the formation of a lake. For the initial conditions, we therefore assume that the Laonong River profile starts at time t_0 from the piecewise linear profile of equation (17), with initial value $z_s(0, t_0) = z_0$ at the confluence, and constant slopes S_U and S_D upstream and downstream. We determine parameters z_0, S_U, and S_D by best fit from the profiles surveyed in August 2004 by the WRA.

[42] Somewhat arbitrarily, we choose the date of 1 May 2007, the beginning of the 2007 typhoon season, as the starting time $t_0 = 0$ of the simulations. Conditions of

Table 3. Measured Time Evolution of Stream Bed Elevation and Water Stage at Selected Cross Sections for the Lake Formation and Decay Experiment Used as a Validation Example

	t (s)										
	0	46	103	157	214	239	268	298	332	365	393
x (mm)	*Stream Bed Elevation z_s (mm)*										
−500	55.5	55.8	56.7	58.9	62.2	63.7	64.9	65.5	66.0	66.4	66.4
−250	26.5	28.7	36.7	36.9	37.0	36.9	37.0	43.1	42.8	42.6	42.5
0	−1.2	23.5	37.1	46.8	54.9	58.5	41.8	33.3	28.0	23.7	21.2
250	−28.1	−20.9	−10.1	−1.4	6.5	10.0	5.7	2.4	−0.6	−2.6	−4.0
500	−54.2	−53.9	−50.2	−44.4	−38.2	−35.5	−34.2	−34.2	−34.5	−34.8	−34.9
x (mm)	*Water Stage z_w (mm)*										
−500	56.9	57.3	58.2	60.7	63.9	65.2	66.6	67.6	67.4	67.9	67.9
−250	27.3	29.9	40.2	49.5	58.3	61.8	48.1	44.8	44.6	44.6	44.4
0	0.2	25.3	39.2	48.3	57.2	60.5	44.3	35.8	30.3	26.2	23.4
250	−26.9	−20.0	−8.3	1.0	8.3	11.7	7.2	4.5	1.9	−0.6	−2.2
500	−52.8	−52.5	−47.4	−42.2	−35.8	−33.6	−32.6	−32.3	−32.7	−33.5	−33.4

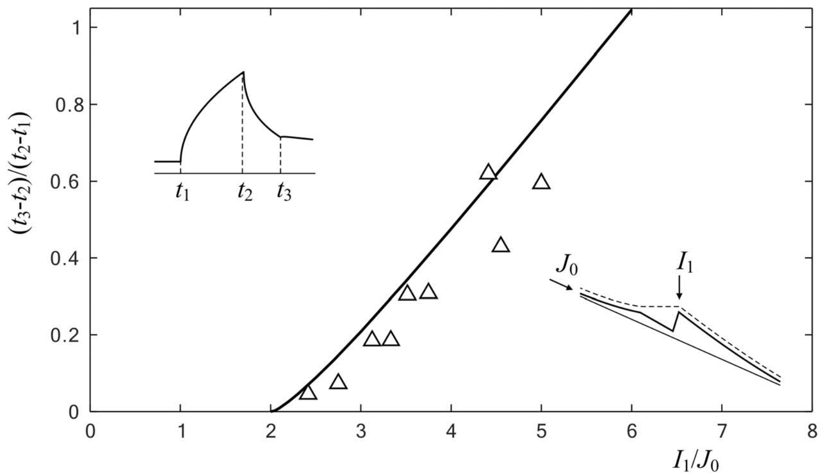

Figure 13. Time to lake elimination (normalized by the duration of lake growth), plotted against the ratio of tributary sediment influx I_1 (during lake growth) to trunk river sediment transit J_0. Solid line, theoretical prediction (computed by finite differences); triangles, experimental measurements for 9 different laboratory runs. Higher rates of tributary sediment influx (or longer lasting lake growth) create larger lakes, which survive longer after tributary influx is terminated.

dynamic equilibrium appear to have prevailed at the confluence prior to the lake formation event. We therefore assume that the initial conditions of our simulations in May 2007 can be approximated by the profiles surveyed in August 2004. We could start simulations instead from the actual date of the 2004 survey, but this would only displace the problem, since we would then have to reconstruct the unknown history of the tributary sediment influx from August 2004 to May 2007.

[43] Information on river flow is more complete. The water discharge hydrograph $Q(t)$ is given by the reconstructed daily streamflow data at Hsing-huei Bridge (section 3.2). For channel width, we adopt the value $B = 90$ m, averaged from 20 transects retrieved from air photographs and checked against widths estimated from our surveyed cross sections. For the normal depth relation (equation (7)), we adopt the rating curve coefficient $C = 0.21$ determined from the depth-discharge relation at Hsing-huei Bridge (section 3.3). The only relationship that is poorly constrained is the bed load transport law $J(Q, S)$, for which no in situ data are available. Earlier studies of river morphodynamics [*Lane*, 1955; *Paola*, 2000] suggest that the simple stream power relation $J = KQS$ obtained by setting $S_{\min} = 0$ in equation (8) is appropriate at field scales. In the absence of more detailed information, we adopt this assumption, and only the transport coefficient K remains to be determined. We retain this coefficient as a free parameter, to be calibrated against the observed river response.

[44] The remaining crucial data gap concerns the time history of the tributary sediment influx, from May 2007 to February 2008. In the absence of any direct measurements or observations of the debris flows responsible for this influx, we adopt for the tributary forcing the simple functional form

$$I(t) = \begin{cases} 0, & t_0 \le t < t_1, \\ \kappa_1 Q(t), & t_1 \le t < t_2, \\ 0, & t_2 \le t. \end{cases} \tag{25}$$

This represents a single period of debris flow activity (possibly approximating the aggregate effect of multiple surges), lasting from time t_1 to time t_2. During this period, the tributary sediment influx is assumed proportional to the water discharge $Q(t)$ in the Laonong River, taken as a proxy for the prevailing hydrological conditions. An alternative would be to use rainfall records, but no gauge is available in the tributary watershed. The morphological response of the tributary dam, moreover, depends more directly on the strength of the tributary influx relative to the trunk river discharge than on either quantity separately. It is therefore convenient to choose as calibration parameter one that exerts the clearest influence on the results. The corresponding dimensionless coefficient of proportionality κ_1 is unknown, as well as the times t_1 and t_2 marking the beginning and end of the sediment influx episode. Three additional free parameters, κ_1, t_1 and t_2, must therefore be adjusted by

Table 4. Experimentally Measured Time to Lake Elimination (t_3) for Different Durations of Lake Growth ($t_2 - t_1$) and Influx Rates J_0 and I of Trunk River and Tributary Sediments, Respectively

	Experiment								
	1	2	3	4	5	6	7	8	9
J_0 (cm^3 s^{-1})	0.26	0.26	0.26	0.26	0.60	0.60	0.60	0.60	0.60
I (cm^3 s^{-1})	0.80	0.90	1.13	1.28	1.45	1.65	2.00	2.25	2.73
t_1 (s)	0	0	0	0	0	0	0	0	0
t_2 (s)	335	273	239	212	349	342	351	266	319
t_3 (s)	397	356	387	338	365	367	416	348	456

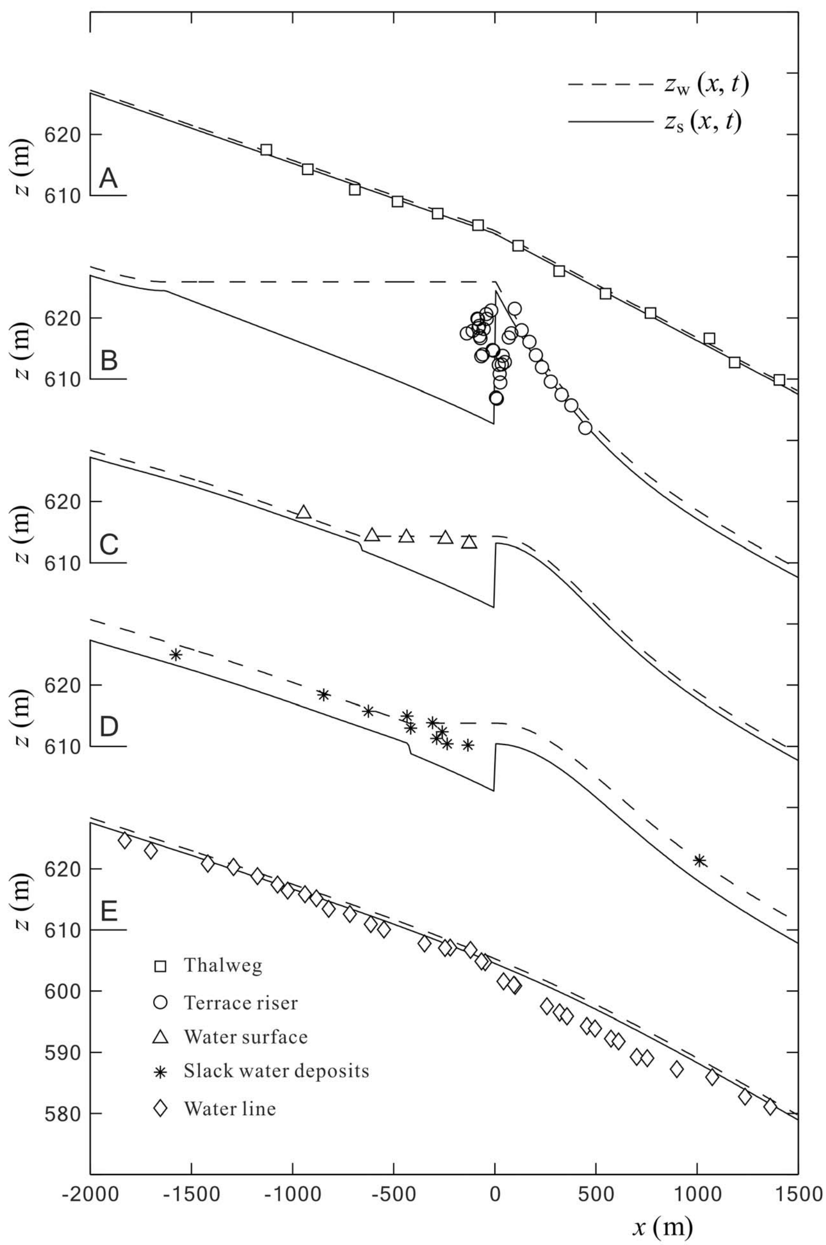

Figure 14. Comparison of simulated and surveyed trunk river long profiles at different stages of the lake life cycle. (a) Before lake formation (t = 0); (b) at maximum dam aggradation (t = 137 d); (c) during lake decay (t = 148 d); (d) at peak discharge of Typhoon Krosa flood (t = 159 d); and (e) after disappearance of the lake (t = 297 d). See Table 1 for relationship between simulation times t and calendar dates.

comparing model outputs with profile data at different stages of the lake life cycle.

6.2. Comparison of Simulated and Reconstructed Long Profiles

[45] Five different river long profiles are available to constrain the simulations (Figures 5b, 5c). First, the profile surveyed by the WRA in 2004 is used to approximate the initial trunk river profile on 1 May 2007. Secondly, the 2007 terrace riser profile surveyed in February 2008 is interpreted as a record of the sediment bed elevation of the trunk river at the time of maximum aggradation. This time is unknown, but coincides in our simulations with the time t_2 of termination of the tributary sediment influx. An additional partial profile is provided by the water surface of the decaying lake on 26 September 2007, estimated from ground photographs. Prior to the elimination of the lake, this is the only profile for which a precise time stamp is available. Next, we interpret the elevations of slack-water deposits along the banks of our surveyed cross sections as points along the high water profile of the last previous flood experienced by the river. This corresponds to the Typhoon Krosa discharge, which peaked on 7 October 2007. Finally, our survey acquired a detailed profile of the low-flow water line on 22 February 2008. The computations were performed with upstream and downstream boundaries at locations $x_U = -5$ km, $x_D = 5$ km, spatial step Δx = 10 m, and variable time step Δt dependent on the

Table 5. Longitudinal Profiles Derived From Field Measurements, Corresponding to Various Stages of the Growth and Decay of the Laonong River Tributary-Dammed Lake (see Figure 14)

Field Measurement													
Thalweg		Terrace Riser				Water Surface		Slack Water		Water Line			
x (m)	z (m)	x(m)	z(m)	x(m)	z(m)	x (m)	z (m)	x(m)	z(m)	x(m)	z(m)	x(m)	z(m)
−1130	617.5	−138	617.5	27	609.4	−945	618.0	−2479	631.4	−2450	628.2	−120	606.7
−925	614.3	−110	617.9	35	612.4	−607	614.3	−1577	625.0	−2322	627.4	−66	604.9
−692	610.9	−86	619.9	39	613.8	−437	614.1	−846	618.4	−2164	627.8	−47	604.7
−482	609.0	−83	619.8	49	612.8	−244	613.9	−625	615.7	−2012	626.6	43	601.6
−282	607.0	−81	618.3	68	616.8	−126	613.1	−434	615.0	−1829	624.6	94	601.0
−83	605.1	−77	618.7	81	617.5			−416	613.0	−1701	622.9	101	600.8
116	601.8	−75	617.0	99	621.5			−308	613.8	−1419	620.8	258	597.5
318	597.7	−72	616.7	133	618.0			−288	611.3	−1292	620.3	320	596.5
547	594.0	−67	613.7	170	616.1			−260	612.4	−1173	618.8	357	595.9
769	590.8	−59	614.0	203	613.9			−236	610.4	−1074	617.4	454	594.3
1061	586.6	−55	618.2	233	611.9			−133	610.2	−1024	616.4	495	593.9
1186	582.7	−43	620.6	276	609.6			1012	591.3	−938	615.8	574	592.3
1407	579.9	−40	619.8	330	607.5					−883	615.2	611	591.8
1573	578.9	−18	621.2	378	605.7					−821	613.5	701	589.2
1678	575.8	−12	614.7	448	602.0					−716	612.6	754	589.0
1831	573.4	−7	614.6							−614	610.9	899	587.3
1949	572.1	5	607.0							−548	610.1	1075	585.9
2049	571.1	10	606.8							−348	607.8	1237	582.7
2154	569.2	19	612.3							−247	607.0	1362	581.1
2255	567.8	24	610.8							−221	607.1		

evolving magnitude of the water discharge, subject to the stability constraint (equation (16)).

[46] As described above, four free parameters had to be calibrated by trial and error: Transport coefficient K, tributary influx coefficient κ_1, and times t_1 and t_2 marking the beginning and end of the tributary influx episode. Because four long profiles are available for comparison (not counting the initial profile used to calibrate S_U, S_D, and z_0), more than enough information is available to constrain these free parameters. We determined their values by seeking the best fit between simulated and observed profiles. Key features targeted during the fitting process include the height and shape of the tributary dam, and the water level in the partially drained lake on 26 September 2007. The trunk river transport coefficient K controls the rate of dam erosion and lake infill during the decay stage. The strength of the tributary influx coefficient κ_1 relative to transport coefficient K controls the shape of the tributary dam at maximum aggradation. Once these are set, the duration $t_2 - t_1$ of tributary sediment influx controls the maximum height reached by the tributary dam. Finally, the water level in the partially drained lake on 26 September is highly sensitive to the time t_2 at which tributary sediment influx is taken to end. We thus find that the calibration parameters can be determined unambiguously, with a significant drop in fit quality if any of them departs from the retained values. Times t_1 and t_2 obtained in this way confirm that the period of high tributary activity coincided with typhoons Wutip and Sepat. The period starts with the arrival of Typhoon Wutip on 8 August 2007 and ends before Typhoon Wipha. Simulations indicate that the tributary dam reached its maximum elevation on 15 September, and that the lake vanished on 23 October. Although the exact timing of the two events is unknown, these dates are consistent with the available field information (see Table 1).

[47] Based on the above reconstruction and calibration, observed and simulated field profiles are plotted in Figure 14. Field measurements are also provided in numerical form in Table 5. The profiles document a lake life cycle that is remarkably similar to the one produced in the laboratory experiments (Figure 11). Starting at time t_0 from an elevation profile that monotonously decreases down valley (Figure 14a), the river bed responds to the tributary sediment influx by forming a temporary dam at the tributary junction. At the time t_2 of maximum aggradation (Figure 14b), the dam crest reaches elevation z_s^{max} = 624.5 m, or about 20 m above the initial river bed elevation z_0 = 603.75 m. The tributary sediment influx which caused this dramatic aggradation is estimated to have lasted $t_2 - t_1$ = 38 days, during which the volume of sediment dumped by the tributary into the Laonong River can be evaluated from

$$\forall_s = \int_{t_1}^{t_2} I(t)dt. \tag{26}$$

This amounts to approximately 980,000 m^3 of bed material (sediment + pore space), or about 1.6×10^6 tons of sediment (dry weight of the granular phase). At the time of maximum aggradation, the simulated lake reached a maximum length L_{max} = 1.6 km, double the length observed during lake decay on 26 September 2007.

[48] Upon termination of the tributary sediment influx, the lake underwent a phase of decay and drainage, characterized by erosion of the lake outlet and lowering of the lake water level. The state of partial lake decay observed on 26 September (Figure 14c) corresponds to a water level which has dropped some 10 m below the maximum lake level. The lake appears to have survived at least until the peak discharge of Typhoon Krosa, on 7 October 2007 (Figure 14d). Under the influence of the peak water discharge Q = 380 m^3 s^{-1}, close to the maximum discharge experienced during the simulation period, the water depth in running-water reaches is estimated to have attained 3.4 m on that date. By the time of our survey on 22 February 2008 (Figure 14e), the lake had completely disappeared, and the river bed approximately returned back to its elevation prior to the episode.

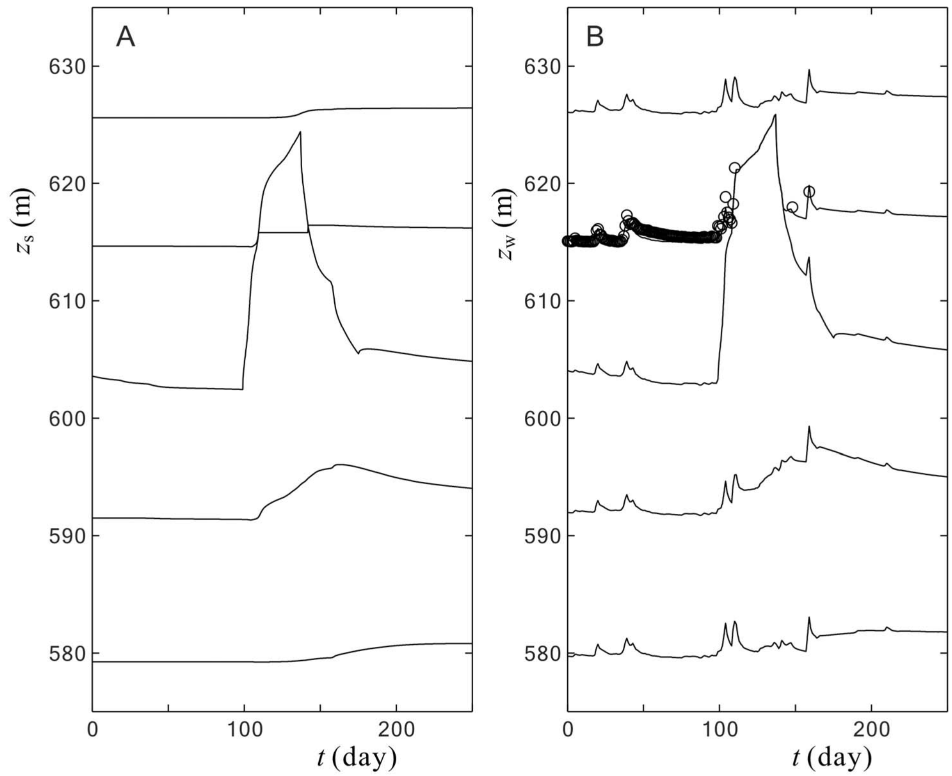

Figure 15. Simulated time evolution of (a) bed elevation and (b) water stage at different cross sections of the trunk river (solid lines), located at positions $x = -1900$, -950, 0, 700, and 1400 m relative to the confluence. Circles in Figure 15b indicate stage measurements at Hsing-huei Bridge.

[49] Through successive stages of lake formation and decay, the simulated and observed profiles (Figure 14) are in good agreement. At the price of four adjustable coefficients, the simulations successfully reproduce the observed river and lake evolution. The agreement generally holds, both upstream and downstream of the confluence, for the entire lake life cycle. An exception is the river bed downstream of the confluence on 22 February 2008 (Figure 14e). Over range $0 < x < 1000$ m, the surveyed profile lies approximately 3 m below the computed profile. Gravel mining activity observed in this area during our survey provides a possible explanation for this difference.

6.3. Elevation Histories and Stage Hydrographs

[50] To further describe the trunk river behavior, Figure 15 shows simulated time histories of the sediment bed and water surface elevations at five different cross sections: One at the tributary junction, two upstream of the junction, and two downstream. The first upstream cross section coincides with the location of Hsing-huei Bridge, and the second downstream cross section is located halfway between the tributary junction and the planned Laonong River weir (see Figure 5). The simulated time histories for the field event (Figure 15) resemble in many ways those obtained for the laboratory experiments (Figure 12). Downstream of the tributary junction, the bed elevation histories track the rise and fall of the tributary dam crest, subject to both delay and attenuation. Upstream of the junction, the sediment bed at Hsing-huei Bridge experienced a delayed rise, a period of constant elevation when drowned by the lake, and then a sudden jump upon passage of the deltaic infill front. This evolution is transmitted, in delayed and attenuated form, to the second cross section further upstream, out of reach of the lake.

[51] For the river sediment bed evolution (Figure 15a), two differences with the laboratory experiments (Figure 12a) can be noted. In the initial stages of the field case, the trunk river acts to diffuse the slope break at the tributary junction, leading to some degradation of the bed prior to the tributary sediment influx. The second difference concerns the appearance of the curves, more irregular in the simulations of the field event. This is due to unsteady variations of the water discharge $Q(t)$, affecting both the bed load transport capacity of the trunk river (via equation (8)) and the rate of tributary sediment influx (via equation (25)). In our simulation of the field event, the water discharge controls the pace of alluvial diffusion and acts as a proxy for the hydrological conditions controlling tributary sediment influx. In the experiments, by contrast, the water discharge and tributary influx (during the period of lake growth) were held constant, leading to simpler curves.

[52] The effect of unsteady water discharge is clearest in Figure 15b, which shows the simulated water surface elevations at the five cross sections. Far from the confluence, fluctuations in water depth are superposed on mildly varying bed elevation variations. The depth fluctuations take the form of asymmetric pulses (receding limb slower than rising limb), mirroring the shape of the water discharge hydrograph (Figure 6). Closer to the tributary junction, the water depth fluctuations are superposed on much greater swings in stage due to the evolution of the tributary dam and lake. The most characteristic response occurs upstream of the junc-

tion, at Hsing-huei Bridge, where the water stage becomes controlled by backwater effects when the cross section is drowned by the lake. Instead of following the local bed elevation, the water stage at the bridge rises and falls with the crest of the tributary dam, 1 km downstream. Due to tributary influence, stage variations driven by river bed aggradation and degradation can therefore greatly exceed those due to fluctuations of the water discharge.

[53] No extended records of sediment bed or water surface elevation are available to verify these simulated histories, except at Hsing-huei Bridge. Daily water stage measurements were recorded there until the bridge deck was submerged on 19 August 2007. After the demise of the bridge, two more data points can be added, one from photographs taken on 26 September 2007, and the other from surveyed slack-water deposits attributed to the Typhoon Krosa discharge peak of 7 October 2007. As shown in Figure 15b, the simulated stage hydrograph at Hsing-huei Bridge exhibits excellent agreement with the measured data. In addition to river and lake long profiles, the simulation can therefore reproduce the complex water stage evolution at Hsing-huei Bridge.

7. Conclusions

[54] In this work, we documented a field example of lake formation and decay, and used the episode to test a simplified mathematical theory of river and lake evolution. Considering the simplicity of the description, we obtained a surprising degree of agreement, showing that the proposed equations can reproduce not only small-scale experiments, but also field-scale processes. For this field application, we found it possible to calibrate the model in a straightforward way, check its results using additional data, and use the simulations to fill in some of the inevitable data gaps. By combining mathematical modeling and field observations, we were thus able to obtain information that neither of these approaches could produce on its own.

[55] According to our analysis, typhoons Wutip and Sepat caused a period of sustained debris flow activity in the Putun-pu-nas River. This led to strong sediment influx into the Laonong River, exceeding the infill capacity of the trunk river and forcing the formation of a lake. During lake growth, the trunk river played a role in shaping the dam-forming deposit. Acting concurrently with tributary influx, streamflow past the dam crest tempered dam growth and diffused the aggradation toward downstream reaches. Upstream of the confluence, meanwhile, sediment transport in the trunk river was interrupted due to the backwater influence of the growing lake. Upon termination of the tributary influx, streamflow from typhoons Wipha and Krosa caused the lake to decay and vanish, by simultaneously incising the dam and infilling the depression. Through these various stages of the lake life cycle, good agreement is registered between observed and simulated profiles.

[56] Associated with this sequence of events, simulated histories of river bed elevation and water stage show considerable complexity. The sediment bed evolution is driven by successive pulses of streamflow, and strongly perturbed by sediment influx from the tributary. The water stage, on the other hand, responds both to slow streambed evolution and to fast fluctuations in streamflow. Due to lake formation, the upstream water stage responds not only to local bed changes, but also to the distant evolution of the dam crest, propagated upstream by backwater influence. As a result, stage records at Hsing-huei Bridge would be impossible to interpret without knowledge of the local and global evolution of the river bed elevation. By taking into account the evolution of water and bed profiles along the entire valley segment, however, we find that the stage record can be accurately reproduced using a relatively simple theory.

[57] Nevertheless, we should caution that the level of agreement obtained may not carry over to conditions distinct from those of semialluvial, steep-sloped Taiwan rivers, evolving due to typhoon floods. If lower flow discharges are of interest, in particular, partial transport conditions may govern the morphodynamic response of the river bed. In that case, it may be necessary to take into account spatial shear stress variations and the differing mobility of separate sediment size fractions. Likewise, for laterally unconfined river segments flowing over alluvial fan surfaces or within wide braiding plains, channel migrations and width variations may exert key influences. Both aspects are disregarded by the present theory.

[58] Various avenues are suggested for future work. First, other case studies should be performed to test, apply, and amend the theory. This could include modeling the Laonong River response to Typhoon Morakot, in August 2009, and trying to anticipate future changes to the valley as it recovers from this record alluviation event. For this and other cases [see e.g., *Blumentritt et al.*, 2009], joint activity and possible river damming by multiple tributaries would need to be addressed. Changes in planform morphology, in addition to long profile evolution, could also be investigated in further experimental and field studies. Finally, more effort is needed to contextualize these recent episodes of tributary activity with respect to the long term evolution of the Laonong watershed.

[59] **Acknowledgments.** Financial support for the present work was provided by the National Science Council, Taiwan, and by National Taiwan University under its Program for Research Excellence. Hydrological and site data were collected with help from Shang-Yao Lien and Shih-Hsien Chang (Southern Region Water Resources Office, Water Resources Agency), and from Chieng-Hsiung Hsiao and Wen-Ming Chen (National Taiwan University). The assistance of Wun-Tao Ke, Yu-Hua Wu, and Shu-Yuan Yang (National Taiwan University) during the 2008 river survey is also gratefully appreciated.

References

Begin, Z. B., D. F. Meyer, and S. A. Schumm (1981), Development of longitudinal profiles of alluvial channels in response to base level lowering, *Earth Surf. Processes Landforms*, *6*, 49–68.

Benda, L., K. Andras, D. Miller, and P. Bigelow (2004), Confluence effects in rivers: Interactions of basin scale, network geometry, and disturbance regimes, *Water Resour. Res.*, *40*, W05402, doi:10.1029/2003WR002583.

Blumentritt, D. J., H. E. Wright, and V. Stefanova (2009), Formation and early history of Lakes Pepin and St. Croix of the upper Mississippi River, *J. Paleolimnol.*, *41*, 545–562, doi:10.1007/s10933-008-9291-6.

Bohorquez, P., and S. E. Darby (2008), The use of one- and two-dimensional hydraulic modeling to reconstruct a glacial outburst flood in a steep Alpine valley, *J. Hydrol.*, *361*, 240–261, doi:10.1016/j.jhydrol.2008.07.043.

Brooks, G. R., and D. E. Lawrence (1999), The drainage of the Lake Ha! Ha! Reservoir and downstream geomorphic impacts along Ha!Ha! River, Saguenay Area, Quebec, Canada, *Geomorphology*, *28*, 141–168, doi:10.1016/S0169-555X(98)00109-3.

Capart, H., B. Spinewine, D. L. Young, Y. Zech, G. R. Brooks, M. Leclerc, and Y. Secretan (2007a), The 1996 Lake Ha!Ha! breakout flood, Québec: Test data for geomorphic flood routing methods, *J. Hydraul. Res.*, *45*, 97–109, doi:10.1080/00221686.2007.9521836.

Capart, H., M. Bellal, and D. L. Young (2007b), Self-similar evolution of semi-infinite alluvial channels with moving boundaries, *J. Sediment. Res.*, *77*, 13–22, doi:10.2110/jsr.2007.009.

Carslaw, H. S., and J. C. Jaeger (1959), *Conduction of Heat in Solids*, Oxford Univ. Press, Oxford, U. K.

Chen, Q., L. Wang, and H. Zhao (2009), Hydrodynamic investigation of coastal bridge collapse during Hurricane Katrina, *J. Hydraul. Eng.*, *135*, 175–186.

Chen, S. C. (1999), Failure mechanism and disaster mitigation on landslide-dammed lakes (in Chinese), *J. Chin. Soil Water Conserv.*, *30*, 299–311.

Costa, J. E., and R. L. Schuster (1988), The formation and failure of natural dams, *Geol. Soc. Am. Bull.*, *100*, 1054–1068.

De Vries, M. (1973), River-bed variations – aggradation and degradation, *Delft Hydraulics Lab. Publ. 107*, 22 pp., Delft, Netherlands.

Fasolato, G., P. Ronco, E. J. Langendoen, and G. Di Silvio (2010), Validity of uniform flow hypothesis in one-dimensional morphodynamic models, *J. Hydraul. Eng.*, doi:10.1061/(ASCE)HY.1943-7900.0000291, in press.

Freeman, W. B., and R. H. Bolster (1910), Surface-water supply in the United States, 1907–1908: Part 9, Colorado River Basin, *Water Supply Paper 249*, 25–26, U.S. Geol. Surv. Reston, Va.

Galay, V. J., D. B. Tutt, and R. Kellerhals (1983), The meandering distributary channels of the upper Columbia River, in *River Meandering*, ed. by C. M. Elliott, pp. 113–125, Am. Soc. Civ. Eng., New York.

Henderson, F. M. (1966), *Open Channel Flow*, Macmillan, New York.

Holmes, A. (1945), *Physical Geology*, Ronald Press, New York.

Hsiau, S. S., J. Smid, F. H. Tsai, J. T. Kuo, and C. S. Chou (2004), Placement of flow corrective elements in a moving granular bed with louvered walls, *Chem. Eng. Process.*, *43*, 1037–1045, doi:10.1016/j.cep.2003.10.006.

Hsieh, M.-L., and S.-J. Chyi (2010), Late Quaternary mass-wasting records and formation of fan terraces in the Chen-yeo-lan and Lao-nung catchments, central-southern Taiwan, *Quat. Sci. Rev.*, *29*, 1399–1418, doi:10.1016/j.quascirev.2009.10.002.

Hsu, J. P. C. (2007), Onset and growth of tributary-dammed lakes across alluvial rivers: Theory and experiments, Master thesis, Grad. Inst. Civ. Eng., Natl. Taiwan Univ., Taipei.

Hsu, J. P. C., and H. Capart (2008), Onset and growth of tributary-dammed lakes, *Water Resour. Res.*, *44*, W11201, doi:10.1029/2008WR007020.

Hutchinson, G. E. (1957), *A Treatise on Limnology*, vol. 1, John Wiley, New York.

Jain, S. C. (1981), River bed aggradation due to overloading, *J. Hydraul. Div., Am. Soc. Civ. Eng.*, *107*, 120–124.

Jones, A. P., H. Shimazu, T. Oguchi, M. Okuno, and M. Tokutake (2001), Late Holocene slack-water deposits on the Nakagawa River, Tochigi Prefecture, Japan, *Geomorphology*, *39*, 39–51, doi:10.1016/S0169-555X(01)00050-2.

Lai, S. Y. J., and H. Capart (2007), Two-diffusion description of hyperpycnal deltas, *J. Geophys. Res.*, *112*, F03005, doi:10.1029/2006JF000617.

Lai, S. Y. J., and H. Capart (2009), Reservoir infill by hyperpycnal deltas over bedrock, *Geophys. Res. Lett.*, *36*, L08402, doi:10.1029/2008GL037139.

Lancaster, S. T., and N. E. Casebeer (2007), Sediment storage and evacuation in headwater valleys at the transition between debris-flow and fluvial processes, *Geology*, *35*, 1027–1030, doi:10.1130/G239365A.1.

Lane, E. W. (1955), The importance of fluvial morphology in hydraulic engineering, *Proc. Am. Soc. Civ. Eng.*, *81*(745), 1–17.

Lin, C. C. (1957), *The Topography of Taiwan* (in Chinese), Taiwan Prov. Doc. Comm., 424 pp., Taipei, Taiwan.

Malavieille, J., and G. Trullenque (2009), Consequences of continental subduction on forearc basin and accretionary wedge deformation in SE Taiwan: Insights from analog modeling, *Tectonophysics*, *466*, 377–394, doi:10.1016/j.tecto.2007.11.016.

Malverti, L., E. Lajeunesse, and F. Métivier (2008), Small is beautiful: Upscaling from microscale laminar to natural turbulent rivers, *J. Geophys. Res.*, *113*, F04004, doi:10.1029/2007JF000974.

Mitchell, N. C. (2006), Morphologies of knickpoints in submarine canyons, *Geol. Soc. Am. Bull.*, *118*, 589–605, doi:10.1130/B25772.1.

Paola, C. (2000), Quantitative models of sedimentary basin filling, *Sedimentology*, *47*, 121–178, doi:10.1046/j.1365-3091.2000.00006.x.

Paola, C., and V. R. Voller (2005), A generalized Exner equation for sediment mass balance, *J. Geophys. Res.*, *110*, F04014, doi:10.1029/2004JF000274.

Ribberink, J. S., and J. T. M. Van der Sande (1985), Aggradation in rivers due to overloading – analytical approaches, *J. Hydraul. Res.*, *23*, 273–283, doi:10.1080/00221688509499355.

Schmidt, A. R., and B. C. Yen (2008), Theoretical development of stage-discharge ratings for subcritical open-channel flows, *J. Hydraul. Eng.*, *134*, 1245–1256, doi:10.1061/(ASCE)0733-9429(2008)134:9(1245).

Schumm, S. A. (2005), *River Variability and Complexity*, Cambridge Univ. Press, Cambridge, U. K.

Shiau, J. T., and F. C. Wu (2009), Regionalization of natural flow regime: Application to environmental flow optimization at ungauged sites, *River Res. Appl.*, *25*, 1071–1089, doi:10.1002/rra.1207.

Soni, J. P., R. J. Garde, and K. G. Ranga Raju (1980), Aggradation in streams due to overloading, *J. Hydraul. Div., Am. Soc. Civ. Eng.*, *106*, 117–132.

Voller, V. R., J. B. Swenson, and C. Paola (2004), An analytical solution for a Stefan problem with variable latent heat, *Int. J. Heat Mass Transfer*, *47*, 5387–5390.

Voller, V. R., J. B. Swenson, W. Kim, and C. Paola (2006), An enthalpy method for moving boundary problems on the earth's surface, *Int. J. Numer. Meth. Heat Fluid Flow*, *16*, 641–654, doi:10.1108/09615530610669157.

Water Resources Agency (1997), Tseng-Wen Reservoir Diversion Project Feasibility Study, Final Report, Water Res. Agency, Taipei, Taiwan.

Water Resources Agency (2007), Laonong weir feasibility study: Gauging station data analysis (in Chinese), Annu. Rep., 11 pp., South. Reg. Water Res. Off., Water Res. Agency, Taipei, Taiwan.

Wright, H. E., Jr., K. Lease, and S. Johnson (1998), Glacial River Warren, Lake Pepin, and the environmental history of southeastern Minnesota, in *Contributions to Quaternary Studies in Minnesota*, *Minn. Geol. Surv. Rep. Invest.*, vol. 49, ed. by C. J. Patterson and H. E. Wright, pp. 131–140, Univ. of Minn., Saint Paul, Minn.

Yang, F.-R., C.-H. Lee, W.-J. Kung, and H.-F. Yeh (2009), The impact of tunneling construction on the hydrogeological environment of "Tseng-Wen Reservoir Transbasin Diversion Project" in Taiwan, *Eng. Geol.*, *103*, 39–58, doi:10.1016/j.enggeo.2008.07.012.

H. Capart and S. Y. J. Lai, Department of Civil Engineering and Hydrotech Research Institute, National Taiwan University, No. 1, Sec. 4, Roosevelt Road, Taipei, TW-10617, Taiwan. (hcapart@yahoo.com)

M.-L. Hsieh, Department of Earth and Environmental Sciences, National Chung Cheng University, 168 University Rd., Minhsiung Township, Chiayi County, TW-62102, Taiwan.

J. P. C. Hsu, Fifth River Management Office, WRA, MOEA No. 123, Cin Shuei Rd., Chiayi City, TW-60065, Taiwan.